

**A SUMMARY OF OBSIDIAN HYDRATION DATING SCIENCE AND METHOD
FOR ARCHAEOLOGISTS**

Alexander K. Rogers, MA, MS, RPA
Maturango Museum, Ridgecrest, CA

Christopher M. Stevenson, PhD
Virginia Commonwealth University

Revised 9/10/2022

Working Paper
MS234A

Abstract

Obsidian hydration dating (OHD) is a method of computing archaeological ages based on measuring water absorption by obsidian artifacts, and is widely used in the desert west. The field has seen significant advances over the past decade, many papers having been published describing advances in the field, but until recently (Rogers and Stevenson 2020) they had not been pulled together to provide a coherent picture in a single place. This paper is an update to that reference, providing a single resource incorporating recent advances for the OHD analyst. We describe obsidian mineralogy as it affects OHD; the effects of structural (intrinsic) water content on hydration; the mathematical form of the hydration law; the mathematics of diffusion theory; the mathematical techniques for controlling for temperature and water content; methods for computing hydration rates; an analysis of error sources; and a recommended method for conducting an OHD analysis. A table of hydration rates for the south-eastern California and southern Nevada region is included. Appendices include a discussion of the mathematics of diffusion, computer codes in MatLab™ for OHD analysis, and a discussion of site formation effects. An accompanying OHD workbook in MS Excel is available on the website of the International Association for Obsidian Studies. We address OHD as currently practiced in the western United States, based on optical microscopy, and do not describe newer, experimental methods such as Secondary Ion Mass Spectrometry or infrared (IR) spectroscopy.

INTRODUCTION

Obsidian hydration dating (OHD) is a method of computing an archaeological age based on measuring the depth of diffused water in the near surface region of obsidian artifacts. Although currently less accurate than radiocarbon dating, it is also less expensive and hence larger data sets are feasible. Unlike dating by projectile point typology, OHD can be applied to debitage as well, and it is the only chronometric method which can directly date obsidian artifacts. It is often the only option for chronometric assessments of sparse desert sites, where radiocarbon or dendrochronology specimens are lacking. Its ability to determine ages for non-diagnostic artifacts makes it useful in studies of trade and exchange, by correlating obsidian compositional and age data from a number of sites. Unlike radiocarbon or dendrochronology, obsidian hydration is primarily controlled by post-depositional processes, especially temperature history, so great care is needed in controlling for environmental effects.

Obsidian hydration dating as a discipline dates from the original paper of Friedman and Smith (1960). They correctly identified the physical process involved and the mathematical form of the hydration law, and other fundamental properties of hydration. Subsequently other advances were made, primarily by researchers in glass science and geochemistry (Shelby 2005; Zhang 2008). Within the field of archaeology, attitudes toward OHD have gone through periods of great optimism (e.g. Friedman and Long 1976; Hull 2001) and of complete disillusionment (e.g. Ridings 1996; Anovitz et al. 1999). In recent years the field of OHD has benefited greatly from the rigorous application of physics, geochemistry, and glass science, so that the basic physics and mathematical models are now understood, and are the basis for the present treatment. The current paper is a revision of Rogers and Stevenson (2020) to incorporate recent advances.

The OHD method described here is based on usual archaeological practice as applied in the western United States. The obsidian specimens are grouped by geochemical source, and a hydration rate is ascribed to the source, but the hydration rate is not adjusted for the individual specimen. Hydration measurements are made by optical microscopy, and temperature and humidity corrections are made by calculation from meteorological records or on-site temperature measurements. An age estimate is generally computed; although recent advances also allow computation of age standard deviation, few analysts do so (for examples including age accuracy, see Rogers and Yohe 2014, 2020).

Analytical methods which are not general archaeological practice at present are not addressed: Secondary Ion Mass Spectrometry (Anovitz et al. (1999, 2004); Liritzis and Laskaris (2012 and references therein); Riciputi et al. (2002); Stevenson et al. 2004); Fourier Transform Infrared spectroscopy (Newman et al. 1986), or Infrared Photo-Acoustic Spectroscopy (Stevenson and Novak 2011).

It is assumed for this discussion that the reader is familiar with the need and technology for geochemical sourcing of obsidian specimen, and with the technique for optical measurement of hydration, so the details of these measurements are not discussed here.

To begin our discussion the mineralogy of obsidian is described as it affects OHD, the mechanics of the hydration process are summarized, and the effect of the intrinsic, or structural, water content on hydration rate is described. This is followed by an overview of the mathematical theory of diffusion to provide a basis for the subsequent discussion of temperature correction and effective hydration temperature (EHT). Computation of EHT requires temperature parameters for the archaeological site, so a method for deriving the parameters using regional

temperature scaling is given; the example is for the Mojave desert of California, but the user can extend the method to other areas as needed. Two techniques are described for computing EHT and the resulting adjustments to the hydration rims.

Age analysis by obsidian hydration requires knowledge of the hydration rate of the obsidian, so seven methods for computing hydration rates are described, with mathematical details. Rates are tabulated for twenty-six obsidian sources likely to be encountered in the eastern California desert area. Finally, the archaeological age analysis process itself is described, including calculation of age accuracy. Computer code in MatLab for age computation is provided, along with a description of a workbook in MS Excel for chronometric analyses. The references cited are not exhaustive, but will provide useful background for those interested.

OBSIDIAN MINERALOGY

Obsidian is an aluminosilicate glass, formed by rapid cooling of rhyolitic magma. Like any other glass, obsidian is not a crystal, and thus it lacks the lattice structure typical of crystals at the atomic level, but it does possess a matrix-like structure exhibiting some degree of short-range spatial order (Doremus 1994:27, Fig. 2; 2002:59-73). Obsidians are typically about 74% silica (SiO_2) and about 14% alumina (Al_2O_3) by weight, the remainder being matrix modifiers (mostly alkaline oxides) and trace elements (mostly rare-earth elements), some of which are source-specific (Doremus 2002:109, Table 8.1; Hughes 1988; Stevenson et al. 1998; Zhang et al. 1997). The trace elements provide the means for geochemical provenance studies. The anhydrous composition (chemical composition independent of water) of obsidians from a wide variety of sources has been shown to be remarkably consistent, within a few tenths of a weight percent (Zhang et al. 1997). The minute interstices within the glass matrix, on the order of 0.1 - 0.2 nanometers in diameter, are where water penetration takes place. Like all glasses, obsidian is physically and chemically unstable and breaks down over long time scales.

All obsidians also contain small amounts of natural water, known as intrinsic water or structural water, resulting from the incomplete degassing of the rhyolitic melt during its ascent from the magma chamber; the amount is generally < 2.5 wt.% in natural obsidians, although cases of somewhat higher concentration are occasionally encountered (Stevenson et al. 2018). It has significant effects on hydration rate, discussed below.

HYDRATION AND ITS MEASUREMENT

“Obsidian hydration”, in its most basic aspect, describes the process by which water is absorbed by obsidian, and involves both physical and chemical changes in the glass (Doremus 2002; Anovitz et al. 2008; Kuroda et al. 2018, 2019; Kuroda and Tachibana 2019). When a fresh surface of obsidian is exposed to air, water molecules adsorb on the surface. Adsorption is a chemical bonding process, distinct from condensation, and the adsorbed layer may be many molecules deep (Kuroda et al. 2018, 2019; Kuroda and Tachibana 2019). Some of the adsorbed water molecules, plus other water molecules impinging directly from the atmosphere, are absorbed into the glass and diffuse into the interstices in the glass matrix. The absorption process occurs when a water molecule has sufficient energy to stretch the glass matrix and enter one of the interstices. Some of the diffusing H_2O molecules react with the silica or alumina in the glass, forming hydroxyl (OH) and causing an increase in volume and openness of the hydrated region. Since the hydrated region is expanded and the non-hydrated region is not, a stress region exists

between the two. The stress region is visible under a polarizing microscope due to stress birefringence. As time passes, the region of increased water concentration progresses into the glass, its rate of progress being a function of the initial openness of the glass, temperature, and the dynamics of the process itself. When the hydrated layer becomes thick enough, typically greater than $\sim 20\mu$, the accumulated stresses cause the layer to spall off as perlite (Friedman et al. 1966).

The depth of water penetration is measured by determining the depth of the stress zone. A thin slice is cut from the margin of an artifact with a diamond saw, mounted on a microscope slide, polished to transparency, and observed under a polarized light microscope (Figure 1).

The thickness of the hydrated layer (the “rim” or “rind”) is on the order of microns, so typically a petrographic microscope system with an optical magnification of 400X or more is used. The rate of hydration can be determined by any of a number of methods (discussed below), the equation relating penetration depth to time is known, and thus age can be computed. The age accuracy, measured by age standard deviation, can also be computed. The resulting ages and standard deviations are accurate enough to place an artifact in the correct archaeological period and answer interesting anthropological questions (Rogers and Yohe 2014).

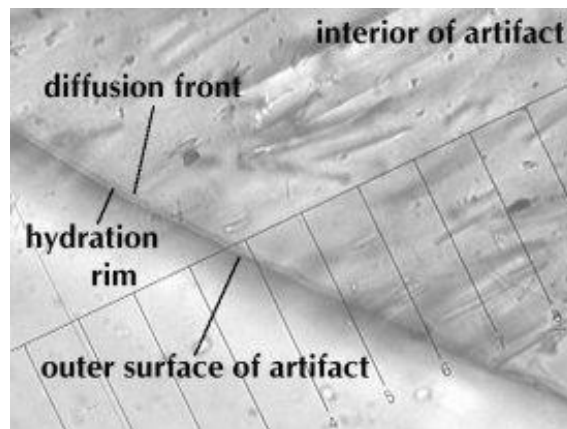


Figure 1. Cross-section of hydration rim measurement, 400X. Photo courtesy of Jennifer Thatcher, Willamette Analytics LLC.

Many forms of the age equation have been published over the years (e.g. Basgall 1990; Bettinger 1989; Friedman and Long 1976; Pearson 1994), but only the equation of Friedman and Long (1976) was based on the physics of the process. Hydration of obsidian is a diffusion process (Doremus 2000, 2002), which, by definition, is a process in which mass is transported due to a concentration gradient (Crank 1975). All laboratory data (e.g. Rogers and Duke 2011; Stevenson and Scheetz 1989; Stevenson et al. 1998; Stevenson et al. 2019) and theory (Crank 1975; Ebert et al. 1991; Doremus 2002) indicate that the position of the stress zone due to hydration progresses into the obsidian such that depth is proportional to t^n , where t is time and $n = 0.5$ within limits of experimental error. Thus the age equation which should be employed is

$$t = r^2/k \tag{1}$$

where t is age in calendar years, r is rim thickness in microns, and k is the hydration rate in μ^2/year (Friedman and Long 1976; Rogers 2007a, 2012a). No other equations for age are valid. If data from an archaeological site seem to conform better to another equation, it is because of experimental errors in the data; archaeological data are not sufficiently accurate to question equation (1) (Rogers 2006).

OBSIDIAN COMPOSITION AND HYDRATION RATE

Obsidian anhydrous chemistry has traditionally been regarded as having a major influence on hydration rate, and attempts have been made to determine a chemical index to predict hydration rates (Friedman and Long 1976; Stevenson and Scheetz 1989). However, Stevenson et al. (1998, 2000) found no consistent influence of anhydrous chemistry on hydration rate. Zhang and Behrens (2000) and Behrens and Nowak (1997) found the effect of anhydrous chemistry to be negligibly small, although Karsten et al. (1982) reported that Ca^{2+} concentration may influence hydration rate to a very slight extent. It now appears that anhydrous chemistry has a negligible effect on hydration rate and attempts to predict hydration rate from anhydrous composition are unlikely to succeed.

Intrinsic water, on the other hand, has a profound affect on hydration rate since it impacts the openness of the glass structure during formation of the glass from a melt (Behrens and Nowak 1997; Delaney and Karsten 1981; Karsten et al. 1982; Lapham et al. 1984; Rogers 2015a; Stevenson et al. 1998, 2000; Zhang et al. 1991; Zhang and Behrens 2000). Shelby (2005:145ff.) describes the effects of adding network modifier molecules such as water to a glass melt. A melt of silica and alumina is a liquid, with no internal order, but as the temperature is lowered the silica-alumina network starts to form. If there are no modifier molecules present, the network forms with the interatomic spacing characteristic of its composition, approximately 0.086 nanometers for silica glass (Doremus 2002:67). If modifier molecules such as water are present the glass has to form interstices around them (Shelby 2005:145); the radius of a water molecule is in the range of 0.138 – 0.233 nanometers (Doremus 2002:63), so the diameter is roughly 0.4 nanometers, which leads to much larger interstices than for the water-free case (Ambrose and Stevenson 2004; Garofalini 2020; Stevenson et al. 2019). These larger interstices represent voids in the glass matrix, which can be more easily penetrated by water molecules. Thus, increasing the structural water content leads to increased hydration rate (Kuroda et al (2018, 2019; Kuroda and Tachibana 2019).

Stevenson et al. (1993) analyzed the intrinsic water content of obsidians from the Coso Volcanic Field source in eastern California. Coso was known to have four geochemically distinct subsources (Hughes 1988), and Stevenson et al. (1993) demonstrated that the mean intrinsic water content of the subsources varied between subsources, and also that there was significant variation within each subsurface. The variation in intrinsic water within a geochemical source or subsurface leads to variations in hydration rate, which in turn increases the uncertainty (statistical error) in computed ages (Rogers 2015a). The effects of these errors have been analyzed in detail in Rogers (2008a, 2010).

From a practical standpoint, controlling for geochemical source acts as a proxy for controlling for intrinsic water (Stevenson et al. 2000), albeit rather poorly (Stevenson et al. 1993; Rogers 2008). Geochemical sourcing controls for the mean value (central tendency) of intrinsic water in the obsidian from that source; the uncontrolled intra-source variation in water content is reflected in the standard deviation of age.

A SUMMARY OF DIFFUSION THEORY

Hydration of obsidian is known as a diffusion-reaction process (Doremus 2000, 2002); in physics, diffusion is a process in which mass is transported due to a concentration gradient, and always follows equation (1). Key points of the mathematical theory of hydration are presented

here to provide the background for discussion of effective hydration temperature. A more complete treatment of the mathematical theory of diffusion is in Appendix A.

The obsidian hydration process is modeled physically as a diffusion-reaction process, which describes the transport of molecular water with time; the diffusion equation is a second-order partial differential equation relating water concentration to depth and time (Crank 1975). A consequence of the mathematical solution to the diffusion equation is that any point on the concentration curve, such as the 50% point, progresses into the obsidian with the square root of time. Depth and time are related by a constant, the diffusion coefficient (D). However, in the archaeological case D is not actually constant, since it is a strong function of temperature, which fluctuates daily and seasonally. The variation of D with temperature is described by the Arrhenius equation,

$$D = A \cdot \exp [-E/(R \cdot T)] \quad (2)$$

where A is a constant with units of length²/time, E is the activation energy of the diffusion reaction in J/mol, R is the universal gas constant (8.315 J/mol °K), and T is absolute temperature in Kelvins (K, where K = °C + 273.15). Thus, since the temperature undergoes both annual and diurnal variation, D varies as well.

However, if D is a function of time only, diffusion can be described by an effective diffusion constant D_{eff} , which is the time average of D over the history of the specimen; it is also the archaeological hydration rate, referred to as k in equation (1). Although temperature varies in a complex manner over time, D_{eff} is determined by a single parameter, the effective hydration temperature EHT. By definition, EHT is a single temperature which yields the same hydration results as the actual varying temperature over the same time. Effective hydration temperature is related to D_{eff} by

$$\text{EHT} = E/[R \cdot \ln(D_{\text{eff}}/A)]. \quad (3)$$

If a time-varying temperature history can be modeled numerically, an effective hydration temperature can be computed by

$$\text{EHT} = -(E/R)/\ln\{(1/N) \sum \exp\{[E/(R \cdot T(t_i))]\}\}. \quad (4)$$

The sum in equation (4) is taken over N data points, encompassing at least one full cycle of the lowest-frequency variation (twelve months, in the archaeological case). The resulting EHT is a rigorous solution for time-varying D.

Equation (4) is important as the basis for computing EHT, which in turn is the basis for controlling for temperature in OHD. Due to the mathematical form of the Arrhenius equation, EHT is always higher than the mean temperature (except in the case of a constant temperature, in which case they are the same). Further discussion is in Appendix A and Rogers (2007a, 2012).

CONTROLLING FOR TEMPERATURE EFFECTS

Effective Hydration Temperature Calculation

Computing EHT by equation (4) requires a mathematical model of the temperature

history for the artifact. The temperature at an archaeological site can be modeled as the sum of a mean temperature and two sinusoids; one with 24-hour period and the other with a 12-month period. The constant term is the annual average temperature, T_a . The sinusoid with a twelve-month period is the annual variation, V_a , and describes the variation of monthly average temperatures through the year. The sinusoid with a 24-hour period is the mean diurnal variation, V_d , describing the daily hot and cold cycle. A technique to determine the amplitudes T_a , V_a , and V_d for any given archaeological site is described below under Temperature Estimation. Temperatures have also varied over longer archaeological time scales, which can introduce an error into age estimates made based on current conditions. A technique to correct for this when necessary is also described below.

For buried artifacts, V_a and V_d must represent the temperature variations at the artifact burial depth, which are related to surface conditions by

$$V_a = V_{a0} * \exp(-0.44z) \quad (5a)$$

and

$$V_d = V_{d0} * \exp(-8.50z) \quad (5b)$$

where V_{a0} and V_{d0} represent nominal surface conditions and z is burial depth in meters (Carslaw and Jaeger 1959:81). (Note that the similar equations in Rogers (2007a, 2012) are incorrect). Depth correction for EHT is desirable, even in the presence of site turbation, because the depth correction, on the average, gives a better age estimate (Rogers 2007b).

The time increment in the temperature data in equation (4) is one hour, and the period of integration is one year. In a practical sense, numerical integration of equation (4) requires a mathematical software package such as MatLab or Mathematica; it can be performed by MS Excel, but, with a 1-hour time increment, it requires a spreadsheet with 8760 lines, which is cumbersome, slow, and prone to errors. Computer code in MatLab to perform the computation is in Appendix B; it will also execute under the Gnu Octave software environment, but the user must still know how to program in MatLab.

Since MatLab is not generally available in the archaeological community, an algebraic best fit was developed for ease of computation. A large number of runs was made with MatLab for temperature parameters typical of archaeological sites, and a best fit equation developed. The resulting equation for EHT, which specifically accounts for average annual temperature, mean annual temperature variation, mean diurnal temperature variation, and burial depth, is

$$\text{EHT} = T_a + 0.0062 * Y \quad (6a)$$

where T_a is annual average temperature, and the variation factor Y is defined by

$$Y = V_a^2 + V_d^2, \quad (6b)$$

in which V_a and V_d are as defined above in equations (5a – b) (note that equation (6a) is a simplification of the corresponding equation in Rogers 2007a and 2012). All temperatures are in °C. For typical desert conditions, equation (6a – b) agrees with the results of equation (4) to within 0.25°C, 1-sigma. Equations 6(a – b) are built into the MS Excel spreadsheet described further below.

Hydration Rim Adjustment for Temperature

Once EHT has been computed, either by equation (4) or equations (6a – b), the measured rim thickness r_m is adjusted to the EHT of the rate by multiplying by a rim correction factor (RCF); the purpose is to adjust the rims to the EHT for which the hydration rate was measured:

$$RCF = \exp\{[(E/R)/(EHT_s + 273.15) - (E/R)/(EHT_r + 273.15)]/2\} \quad (7)$$

where E and R are defined as above, EHT_s is the EHT computed for the specimen, and EHT_r is effective hydration temperature for which the hydration rate was computed, both in °C. The EHT-adjusted rim value r_c is then

$$r_c = RCF * r_m \quad (8)$$

The value r_c is then used in equation (1) to compute age. Further, the EHT-adjusted rim standard deviation is

$$\sigma_c = RCF * \sigma_m \quad (9)$$

where σ_c is the corrected standard deviation and σ_m is the standard deviation as measured by the OH laboratory.

Inferring Activation Energy

Values of E/R for obsidians range from ≈ 9000 K to ≈ 11000 K (Friedman and Long 1976). Rogers and Stevenson (2021, n.d.) reported an equation relating hydration rate to intrinsic water content and temperature, discussed below under Intrinsic Water Calibration. This equation can be rearranged to yield an equation for activation energy of

$$E/R = T*[36.29 - \ln(k)]. \quad (10)$$

where T is in Kelvins. Thus, once hydration rate is computed, the corresponding value of activation energy can be determined for use in hydration rim adjustments (equation (7)); failing this, a value of $E/R = 10,000$ K is recommended.

Effects of Site Formation Processes

Site formation processes, including turbation due to biological, geological, or climatic effects, are well known (Schiffer 1986). The EHT that an obsidian artifact is exposed to is a strong function of burial depth, and, for deeply buried artifacts, can significantly affect the age computed by OHD, since temperature variations decrease with depth. Computing age based on higher temperature surface conditions and ignoring the effects of burial depth will invariably yield an age which is too young. On the other hand, if the burial conditions have changed significantly over time, computing age based on the recovery depth may yield ages which are too old; an example of the latter would be deeply buried artifacts eroding out of a dune field.

The method for accounting for changes in depth is time-averaging, whose physical basis is that the overall hydration rate is the time-average of the instantaneous rate, over the temperature history of the artifact (equation (4), above). Note that this is not the same as the hydration rate for the average temperature, nor the hydration rate for the average depth. It is immaterial whether the artifact is buried and then exposed or vice versa (Duke and Rogers 2013). The principle is to compute the hydration rate at depth and on the surface, and then compute a weighted average based on what fraction of its life the artifact was buried. The computer code in Appendix B accounts for the length of time an artifact was buried, as well as the depth, based on a user-input value of the fraction of that artifact life that it was buried. The algorithm computes an average value of the diffusion coefficient over time and uses this value to compute age. The standard deviation of computed age due to site formation is the difference of the two limiting ages (surface and depth) divided by $\sqrt{12}$; its effect is included as shown in equation (39).

When computing age by MS Excel, the age corresponding to the average hydration rate is

$$t = r_m^2 * [Y/RCF_d^2 + (1 - Y)/RCF_s^2] / k_z \quad (11)$$

where r_m is the measured rim value, k_z is the hydration rate at temperature EHT_z , Y is the fraction of the artifact's life that it was buried, RCF_d is the rim correction factor for the EHT at depth relative to EHT_z , and RCF_s is the rim correction factor for the EHT at the surface relative to EHT_z . If no other information is available, a value of 0.5 is recommended for Y . The derivation is in Appendix C.

Temperature Parameter Estimation

Temperature parameters can be computed from meteorological records or from on-site temperature sensors. It is important to use long-term data in these computations, and 30 years is the standard for determining climatological norms (Cole 1970).

Meteorological Data

Meteorological data are available at no cost from the Western Regional Climate Center (WRCC). Two cases are discussed here: the situation in which there is a meteorological station near the archaeological site, and the situation where there is not. In each case an example is given to illustrate the process.

If there is a nearby meteorological station, data from the station can be downloaded from the WRCC website (www.wrcc.dri.edu) and used as a proxy for conditions at the site. As an example, the Rose Spring site (CA-INY-372) is within a mile of the power plant at South Haiwee Dam and at the same elevation, which provides a data set which can be copied and pasted into an MS Excel spreadsheet from the WRCC website. The temperature data are reported in °F, so the first step is to convert to °C ($^{\circ}C = 5 * [^{\circ}F - 32] / 9$). Next the overall average is computed, which is T_a . The average for each month is then computed, and V_a is the hottest month mean minus the coldest month mean (typically August minus January). Finally the diurnal range is computed, and its mean is V_d . With T_a , V_a , and V_d known, the EHT can be computed.

Unfortunately, many archaeological sites are not collocated with meteorological stations and furthermore, there may be considerable variations in elevation which affects temperature. In such a case, typical of much of the desert west, temperature parameters can be estimated by regional temperature scaling. The scaling principle is that desert temperature parameters are a strong function of altitude above mean sea level, (amsl) and the estimates of temperature can be

determined by scaling from 30-year data from large a number of meteorological stations. An example is presented from the upper Mojave desert.

The analysis is again based on monthly temperature data from the Western Regional Climate Center. Fourteen meteorological stations were used, ranging from 940 to 11,470 ft amsl. In each case the data were downloaded from the WRCC website and parameters computed as shown for the Haiwee case above. Table 1 shows the data.

Table 1. Temperature parameter data, upper Mojave Desert

Site	Altitude, ft	T _a , °C	V _a , °C	V _d , °C
Baker	940	21.27	25.25	17.55
Trona	1700	19.29	24.36	16.31
Daggett Airport	1930	19.72	22.56	15.63
Cantil	1960	17.88	23.08	18.30
Barstow	2140	17.71	21.58	18.20
China Lake NAF Armitage Field	2240	17.68	23.78	18.12
Inyokern	2440	17.70	21.94	18.50
Mojave	2740	17.13	21.44	14.37
Haiwee	3282	15.38	22.31	15.02
Randsburg	3570	17.03	21.47	13.62
Wildrose	4100	14.86	21.53	14.93
Bishop	4150	13.37	21.92	20.46
Mountain Pass	4700	14.39	22.06	13.60
White Mountain 2	12470	-2.51	16.94	9.48

The expected form of the best-fit scaling equation is $y = a + b \cdot h$, where y is the temperature parameter, a is the y-intercept, b is the slope (known meteorologically as the lapse rate), and h is altitude. The best fit equations can be computed easily with MS Excel, with results as in Table 2.

Table 2. Temperature scaling, upper Mojave Desert

Parameter	y-intercept, °C	Slope, °C/ft	R ²
T _a	22.71	-0.0020	0.9814
V _a	24.25	-0.0006	0.7949
V _d	18.49	-0.0007	0.5178

Thus, temperature parameters for any site in the upper Mojave desert can be predicted based on site altitude. Effective hydration temperatures computed based on the model agree with those from the stations to within 0.63°C, 1-sigma.

These equations are for air temperatures. Obsidian on the surface is exposed to surface temperatures, which can be significantly higher than air temperatures in areas devoid of vegetation (Johnson et al. 2002; Rogers 2008b). However, a detailed analysis based on data from Rose Spring (CA-INY-372) has shown that meteorological air temperature gives a good estimate of surface ground temperature in situations in which even intermittent shade is present (Rogers 2008c). In regions entirely void of vegetation, temperature sensors may be needed to measure ground temperatures.

Caves and rockshelters affect the annual and diurnal variation to a significant degree. Temperature sensor measurements performed in Ray Cave (CA-INY-444) showed that the annual variation (monthly mean for hottest month minus monthly mean for coldest month) inside the cave was about 75% of the variation outside. For archaeological calculations, V_a can be determined by a meteorological model and then multiplied by 0.75. Diurnal variation within

caves has been measured to be approximately 5°C, year around (Everett-Curran et al. 1991).

Temperature Sensors

Temperature sensors at a site are sometimes necessary for determining temperature parameters, but must be used with care. Today, digital sensors such as Hobo™ or iButton™ sensors are available at very low cost and are the preferred method for measuring temperature. Such devices incorporate both a sensor and a data logger, and can be set to sample temperatures at any desired hourly interval. Sensors should be placed at the site and left undisturbed for a year, then removed and down-loaded. The temperature parameters can be computed from the data set (Rogers 2008b), or the data stream can be used as direct input to equation (4).

A caveat is that temperature sensors do not represent 30-year data, which is the meteorological standard for long-term conditions (Cole 1970). Sensor data should be compared with meteorological records to ensure that any difference is due to conditions at the site and not to an anomalous year.

Paleotemperature Effects

The parameters which characterize the current temperature regime, whether determined by use of sensors or meteorological records, are a reasonable approximation to ancient temperatures for ages in the Holocene. However, multi-proxy data have been published which show significant shifts in ancient temperatures relative to the present (e.g. Bintanja et al. 2005; West et al, 2007), especially for ages before approximately 12 - 13Kya (Figure 2).

Data sources include marine fossils, tree-ring data, studies of *Neotoma* nest contents, pollen records, and Greenland ice cores (Bintanja et al. 2005; West et al, 2007). For these ages the prevailing temperatures were significantly cooler than today, and ages computed assuming current conditions will be too young.

The key parameter in temperature studies of obsidian is EHT, rigorous computation of which requires all three of the temperature parameters. These can be easily determined for current conditions, but the situation is different for ancient climates. As described above,

the published temperature summaries such as seen in Figure 2 are based on proxy data, and represent changes in mean annual temperatures; however, similar proxy data showing how annual and diurnal temperature variation have also changed over time have not been published. However, changes in both annual mean temperature and the annual and diurnal temperature variations are driven by the same mechanism: changes in insolation caused by changes in the

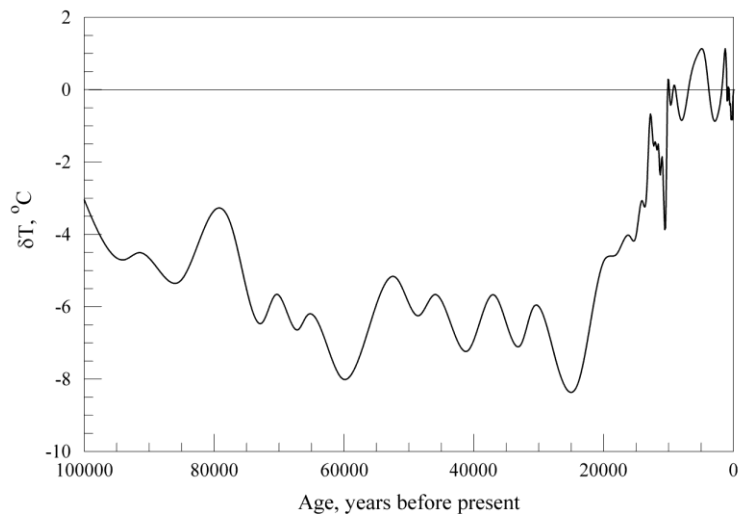


Figure 2. Changes in north temperate zone mean temperatures since the mid-Pleistocene reconstructed from multi-proxy data by Stineman interpolation (Bintanja et al. 2005; West et al. 2007:17, Fig. 2.2).

earth's orbit; thus, it is likely that the annual and diurnal temperature variations have varied in proportion to variations in average annual temperature. By this model, the change in EHT over geologic time scales can be represented by the change in mean annual temperature.

Rogers (2015b) reported an analysis of the effects of paleotemperature shifts on OHD, based on temperature proxy data back to 200Kyr, and on the assumption that any changes in EHT over time are equivalent to changes in mean temperature. It was found that the effects of paleotemperature shifts on hydration rate are negligible for ages less than about 13,000 years; for earlier ages a correction should be applied. Details of the analysis and correction method, including spreadsheet and MatLab tools, are in Rogers (2015b).

Humidity Effects

Ebert et al. (1991) and Friedman et al. (1994) reported that the hydration rate, measured by steady-state mass gain, is affected by relative humidity. Mazer et al. (1991), using optical microscopy, reported that the hydration rate increased by a factor of approximately 1.2 between 90% and 100% relative humidity, but was relatively unaffected by humidity if humidity was under about 80%.

Clearly, there is an effect. Unfortunately, humidity trends, unlike temperature trends, are highly random and are virtually impossible to model deterministically, so they can only be incorporated statistically. Interstitial soil humidity is typically > 95%, even in deserts, for depth greater than about 20 cm. (Campbell 2021). The model implemented here assumes humidity varies randomly between 90% and 100%, so the reported factor of 1.2 in rate corresponds to a coefficient of variation of about 6% in rate ($= 0.20/\sqrt{12}$). This factor is included in the MatLab code in Appendix B, but was not included in the code documented in Rogers 2018. It is included in the MS Excel workbook and in the accuracy model described below in equation (36) of this paper.

Temperature Model Validity

The temperature model used for computing EHT is fairly simplistic: a constant term plus two sinusoids, one of 12 month period and the other of 24 hour period, with no adjustment for annual variation in length of daylight hours. An analysis was performed to validate the model against field data, using three years of temperature data from the USGS Amargosa Desert Research Site at Beatty, Nevada; data were from Johnson et al. (2002). The approach was to compute temperature parameters from the data stream and construct a temperature model; the model was then used in equation (4) to compute EHT. In parallel, EHT was computed from equation (4) directly using the sensor data stream as the temperature model. Agreement within 1°C was obtained, and so the model is deemed adequate for archaeological use (Rogers 2008b).

Cautionary Points

Three phenomena can damage an obsidian specimen and thereby affect the validity of an OHD analysis: chemical erosion, mechanical erosion, and heat. Chemical erosion has been discussed by Morgenstein et al. (1999) for the case of soda-lime glass. Using scanning electron microscopy (SEM), they found that water containing Na⁺ and K⁺ ions caused erosion of the glass surface. Although data are lacking for obsidian, it is chemically similar to soda-lime glass and such erosion is possible. It would be most likely to occur in extreme chemical conditions

such as dry playas, but the phenomenon has not been reported archaeologically. If it were occurring it would result in a diffuse hydration front, which would be reported by the OHD laboratory.

Mechanical erosion occurs primarily due to wind-blown sand in desert regions and beach dune deposits. In severe cases the abrasion can obliterate the surface layer of the obsidian. If an internal step-fracture can be located on the specimen, a valid rim may be identified within a internal fissure and the protected hydration layer measured. It is possible that rapidly-flowing, sediment-laden water could cause the same erosion, but it has not been reported.

Since obsidian hydration is a temperature-dependent process, OHD is affected by post-depositional heat exposure of a specimen. Sustained, intense fires, such as forest fires or camp fires in excess of 400°C, will make the hydration rim unreadable, and in extreme cases will destroy the specimen (Steffen 2005). However, lower temperature grass fires typically have no effect. The OHD laboratory will be able to detect fire effects on obsidian, since it usually causes a diffuse hydration rim. Also, obsidian, unlike crypto-crystalline silicates, cannot be heat-treated to enhance flaking. The effect of heat-treating of cherts is to cause vitrification of the material, which fuses the crystalline grains into a glass; since obsidian is already a glass, heat-treating has no benefit and may destroy the specimen (Steffen 2005).

HYDRATION RATE DETERMINATION METHODS

The hydration rate at a known temperature is the other key parameter needed for OHD. Hydration rates can be estimated by any of a number of methods, the most common of which are radiocarbon association, temporally-sensitive artifact association, artifact baselining, laboratory induced hydration, intrinsic water calibration, curve re-fitting, and inter-method proportionality. Each technique is described below.

Radiocarbon Association

The classic method for computing a hydration rate is by obsidian-radiocarbon association (Basgall 1990). The principle is to measure the hydration rims for a number of obsidian specimens from contexts of different time periods that are associated with radiocarbon-dated organic materials. The underlying assumption of the method is that the obsidian and radiocarbon entered the archaeological record at approximately the same time. The obsidian layer thicknesses are then adjusted to a common EHT value (equations [6] and [8], above), and a least-squares best fit computed to the calibrated radiocarbon data. A hydration rate can then be computed based on equation (1).

Obsidian specimens for inclusion in hydration rate computation should be selected with care. First, they must be geochemically analyzed, and segregated by geological source in order to control for the variation in structural water content that can impact the rate of hydration. Second, they should be from a known archaeological provenience; in particular, site temperature regime (or its proxy, elevation) and specimen burial depth should be known, since both affect the EHT computation. Finally, it is wise to document carefully which specimens are used in the computation, with full and careful citation of published documents so the data are traceable.

Prior to use in rate computation, all obsidian readings from each geological source must be adjusted to a common EHT, which includes the effects of site temperature regime and specimen burial depth. In the California desert, 20°C is an appropriate standard EHT, while in

cooler climates such as Oregon, 12°C is typically used (J. Cowan, pers. comm. 2019). Whichever value is chosen, all hydration rims must be adjusted to it, both in rate computation and in age calculation. The mathematics to make the adjustment were fully described above.

Radiocarbon specimens should also be selected with care. Dates from stationary features such as hearths are the best, since they are not normally affected by bioturbation, and obsidian specimens should be stratigraphically linked to the feature. Radiocarbon ages should always be converted to calibrated years, using one of the standard packages such as OxCal or Calib; since most of the obsidian work has been done closer to the year 2000 than to 1950 (the radiocarbon "present"), it is preferable to use 2000 as the present. Ages in this system are calibrated years before 2000, or cyb2k (cyb2k = RC-calibrated age + 50). In some cases involving late prehistoric specimens, adjustment to 2020 may be preferable; in any case, the age reference point should be clearly stated.

The decision of which ages to associate with the rims is often a matter of judgment about the integrity of archaeological context and its impact on the strength of the obsidian/radiocarbon sample association. This situation is frequently the major source of uncertainty in the calculated hydration rate. In particular, it should be borne in mind that the obsidian is likely to migrate vertically within a site, either by bioturbation or by human reuse of obsidian debitage, so the association with radiocarbon dated samples may be spurious. Establishing an association between obsidian and radiocarbon samples is always a matter of detailed observation and interpretation.

It is well known that the development of the hydration rim in obsidian proceeds as described by equation (1) above, so either r^2 vs. t or r vs. \sqrt{t} will yield a straight line. The hydration rate is a slope, and can be computed by least-squares best fit methods. The physics of the situation (zero rim at zero time) dictates that the best fit line must pass through the origin, and the slope is related to the hydration rate. Consider a general data set of N pairs $\{x_i, y_i\}$, in which the y_i values are assumed to include random errors and the x_i values are assumed error-free; the assumption that the independent variable is error-free is a fundamental aspect of least-squares fitting, which is met to a greater or lesser degree with real data sets. (Cvetanovic et al. 1979; Meyer 1975). Assume further that a theoretical model suggests a linear relationship between the two, and that the best fit line is constrained to pass through the origin as in equation (1). The least-squares best fit method then yields a slope of

$$S = \frac{\sum w_i x_i y_i}{\sum w_i x_i^2} \quad (12)$$

(Cvetanovic et al. 1979:52, eq. 6), which minimizes the mean-square errors in y . Here the sums are taken over all N data points, and w_i is a weighting factor, typically chosen to be $1/\sigma_i^2$, where σ_i is the standard deviation of the errors in y associated with the i^{th} data point. Note that σ_i is not the difference between the i^{th} data point and the best fit line.

In applying equation (12), it is possible to choose either time (t), \sqrt{t} , rim value (r), or the square of the rim value (r^2) as the independent variable x . The best fit procedure is based on the assumption that the independent variable is error free, which is clearly not the case here, since there are errors (i.e. uncertainties) in both the hydration rim value and the assumed age. However, the uncertainties in t are dominated by the association problem, so they are typically much greater than uncertainties in r , so t is not a good choice for the independent variable.

Choice of r as the independent variable and \sqrt{t} as the dependent variable minimizes the errors associated with the rate estimate, and is the recommended approach, so the mean value of the hydration rate is

$$k = 1/S^2 \quad (13)$$

Once S has been computed, the next step is to compute the standard deviation of the slope. The best-fit value of y_i (designated \hat{y}_i) is then given by

$$\hat{y}_i = Sx_i \quad (14)$$

The error between the best fit and the measured data is then

$$\delta_i = \hat{y}_i - y_i \quad (15)$$

Finally, the standard deviation of the slope value S is (Cvetanovic et al. 1979:52, eq. 6e)

$$\sigma_S = \sqrt{\sum w_i \delta_i^2 / [(N-1) \sum w_i x_i^2]} \quad (16)$$

and the CV_s of the slope is σ_S/S . The CV of the rate is $CV_k = 2 \times CV_s$, and the standard deviation of the rate is then

$$\sigma_k = CV_k * k = 2 * CV_s * k \quad (17)$$

Appropriate values for the weighting factors w_i must also be defined. If each data point is comprised of an average of N_i values, then $w_i = N_i$; otherwise, $w_i = 1$ is the default value unless there is an *a priori* reason to place greater weight on particular data points.

Thus, given a set of data points and a model of the physical process, the mean and standard deviation of the hydration rate can be computed. Accuracies of 5% are achievable with this method, (Rogers 2010) with the association problem being the chief source of uncertainty.

Temporally-Sensitive Artifact Association

If radiocarbon data are not available, a rate can often be computed based on temporally-sensitive artifacts, particularly projectile points. The use of temporally-sensitive artifacts is not a new approach (e.g. Pearson 1995), but the process is fraught with peril. Should the analyst use the median age for each point type, or try to determine transition points between types? Is the use of either the median or the transition points applicable for very long-lived types such as Elko? Does including long-lived point types improve or degrade the rate estimate?

The method described here addresses these issues by including a confidence-based weighting factor for each data point (Rogers and Duke 2014a). The weighting factors are not arbitrary but are based on the inverse of the known age span of the artifact type; the longer the span, the lower the confidence in the artifact's true age. The analysis assumes the hydration rim data have been corrected for effective hydration temperature (EHT) using the method described above, including the effects of site elevation, burial depth of the artifact, and site formation processes.

The mathematical method for this approach is the same as that for radiocarbon association, except that now values for the weighting factors w_i must also be defined that are appropriate for temporally-sensitive artifacts. The age assigned to a particular artifact is typically the mean or median age for the type. For example, the Rose Spring point is generally considered to have been manufactured between approximately 1600 cal BP (Yohe 1992, 1998) and 650 cal BP (Justice 2002:321); by contrast, the Elko point type was exceptionally long-lived, from approximately 7800 cal BP to 1800 cal BP (Smith et al. 2013:588, Fig. 3). Thus the Rose Spring type would be assigned an age of 1125 cal BP, and the Elko 4800 cal BP.

However, the confidence associated with these ages differs, since the Rose Spring was manufactured over a span of only 950 years, while the Elko span was 6000 years; the shorter the span, the higher the confidence, so the weighting factor should be inversely related to the time span. A simple form for the weighting factors is

$$w_i = 1/(t_b - t_e)^2 \quad (18)$$

where t_b is the beginning age for a given point type and t_e is the ending age. (Strictly speaking, the denominator of equation [18] should be divided by $\sqrt{12}$, to give the standard deviation; however, any constant factor cancels out of equation (12), so the simpler form of equation (18) gives the same slope value). Thus, the mean and standard deviation of the hydration rate can be computed by using the weighting factors from equation (18) in the best fit process described for radiocarbon association.

Hydration rates computed by this method will probably be less accurate than those developed with radiocarbon dates because of the greater age uncertainties connected with projectile point forms. In addition, artifact time spans will differ between the eastern and western Great Basin, and are subject to differences in published artifact typology. However, sometimes this is the only method available to establish chronological control over an archaeological deposit.

Artifact Baselineing

If two temporally-sensitive obsidian artifacts of the same type but different geochemical sources are recovered from the same context at a site, and the rate is known for one of the sources, the rate for the other source can be computed since the hydration rates are proportional to the square of the rim readings. The caveat, of course, is the assumption that the two sources were exploited at the same time.

As an example we look at the Tulare Lake Wide-Stemmed points from the Witt Site (CA-KIN-62) in the San Joaquin Valley of California (Rogers 2012b). The projectile points were all of the same type, and were recovered in the same context. One set of points was sourced to Coso West Sugarloaf (WSL), the other set to Casa Diablo Sawmill Ridge (CDSR). The hydration rate for WSL is known ($18.14 \mu^2/1000 \text{ yrs @ } 20^\circ\text{C}$) (Rogers 2015a), so the hydration rate for CDSR can be computed analytically by assuming that the projectile points were manufactured at approximately the same time, irrespective of obsidian source; that they experienced similar temperature histories; and that the growth of the hydration rim is proportional to the square-root of time.

The analysis is based on equation (1), which is $r^2 = k*t$, where r is the hydration rim measurement, t is age, and k is the hydration rate. If we assume that the points are of the same

age, regardless of obsidian source, that they have experienced the same temperature history, and that we know the hydration rate of one source such as WSL, then the hydration rate of any other source such as CDSR is

$$k_{\text{CDSR}} = k_{\text{WSL}} \times (r_{\text{CDSR}}/r_{\text{WSL}})^2 \quad (19)$$

For the particular case in point, this led to a rate for CDSR of $12.70 \mu^2/1000 \text{ yrs @ } 20^\circ\text{C}$.

There is a major caveat to this method. In addition to the assumption of the same temperature history, it makes an implicit cultural assumption that the two obsidian sources were exploited roughly contemporaneously. In the case of the Tulare Lake Wide-Stemmed points from the Witt Site, the CDSR hydration rate yields archaeologically reasonable ages when applied to other sites and contexts, so this cultural assumption is probably valid. By contrast, when this method was applied to two obsidian sources recovered at Bonneville Estates Rockshelter in western Utah, it did not work (Rogers and Duke 2018); subsequent analyses showed the two sources (Brown's Bench and Topaz Mountain) had been exploited at significantly different times, which invalidated the method (Rogers and Duke 2018) Thus, this method must be treated with caution, and resulting rates cross-checked for validity.

Laboratory Induced Hydration

Theory of Accelerated Hydration

This technique takes advantage of the known temperature-dependence of the hydration process (equation (2)). In this method the rate of hydration is measured at elevated temperatures, where the reaction occurs within weeks instead of millennia, and then adjusted to reflect archaeological temperature. An analysis starts by combining equations (1) and (2) to yield

$$r^2/t = A \cdot \exp[-E/(R \cdot T)] \quad (20)$$

Taking the natural logarithm of each side gives the so-called logarithmic Arrhenius equation

$$\ln(r^2/t) = \ln(A) - E/(R \cdot T). \quad (21)$$

If we define

$$y = \ln(r^2/t) \quad (22)$$

and

$$x = 1/T, \quad (23)$$

equation (21) becomes a linear equation of the form

$$y = I + Sx \quad (24)$$

with $I = \ln(A)$ and $S = -E/R$ (Figure 3).

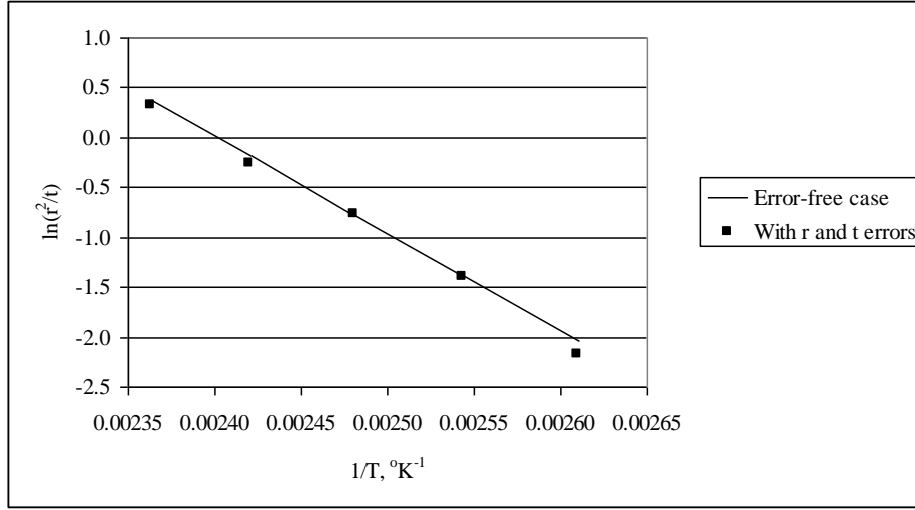


Figure 3. Illustration of a log-Arrhenius plot for laboratory induced hydration. Slope = $-E/R$ and y-intercept = $\ln(A)$.

Given data for r , t , and T for three or more points, equation (24) can be solved as a weighted least-squares linear best-fit not constrained to pass through the origin (Cvetanovic et al. 1979; Meyer 1975); S is the slope and I is the y-intercept given by

$$S = \{\sum w_i \sum w_i x_i y_i - \sum w_i x_i \sum w_i y_i\} / D \quad (25a)$$

$$I = \{\sum w_i x_i^2 \sum w_i y_i - \sum w_i x_i \sum w_i y_i\} / D \quad (25b)$$

and

$$D = \sum w_i \sum w_i x_i^2 - (\sum w_i x_i)^2 \quad (25c)$$

Finally, the slope value S is the negative of the activation energy E/R , and A , the pre-exponential or diffusion constant, is given by

$$A = \exp(I) \quad (26)$$

The parameter w_i is the weight factor for each data point, given by $w_i = 1/\sigma_i^2$, where σ_i^2 is the variance in the y-dimension associated with the i^{th} data point (Cvetanovic et al. 1979). For the functional form $y = \ln(r^2/t)$ it can be shown by the theory of propagation of errors that appropriate weight factors are given by $w_i = 1/((2CV_r)^2 + CV_t^2)$, where CV_r and CV_t are the coefficients of variation for r and t respectively (Cvetanovic et al. 1979; Taylor 1982: 179ff.).

For this analysis the value of CV_r is computed from the hydration rim values in microns measured by the laboratory. The value of CV_t is estimated from laboratory procedures, by assuming that the hot-soak time might vary from an exact number of days by up to an hour or so due to heat-up and cool-down time, or about 0.05 days. The standard deviation of the uncertainty is then $0.05/\sqrt{12}$, which is then used in computing CV_t .

A final source of experimental error lies in the temperature controller for the laboratory oven used for the hot soak. Typical laboratory thermostat controllers are accurate to about $\pm 1^\circ\text{C}$. It can be shown that this adds a temperature increment of 0.06°C to the nominal temperature of the controller; this increment is always positive, not random.

The linear best fit in equations (25a – c) provide best estimates for the mean values of activation energy (E), diffusion constant or pre-exponential (A), and hydration rate. Uncertainties associated with these mean values are characterized by the standard deviations of the activation energy and diffusion constant, which are, respectively,

$$\sigma_E = \sigma\{\sum w_i/D\} \quad (27)$$

and

$$\sigma_A = A*\sigma\{\sum w_i x_i^2/D\} \quad (28)$$

with D defined in equation (25c) and σ given by

$$\sigma = \{\sum w_i(y_i - \hat{y}_i)^2/(N - 2)\}^{1/2} \quad (29)$$

Here x and y are defined as above, \hat{y}_i is the best-fit value of y_i computed from equations (25a-c), and N is the number of data points. The parameter σ is known as the “external or *a posteriori* standard deviation” (Cvetanovic et al. 1979:52).

Computation of the standard deviation of the hydration rate is more complicated because there is a strong cross-correlation term in the errors. If there were no cross-correlation, the standard deviation of the rate σ_{knc} would be simply

$$\sigma_{knc} = \text{sqrt}(\sigma_E^2 + \sigma_A^2) \quad (30)$$

Monte Carlo simulation studies have shown that the effect of the cross-correlation is to reduce the error in rate relative to equation (30), such that the error including cross-correlation σ_k is

$$\sigma_k \approx 0.32* \sigma_{knc}. \quad (31)$$

Laboratory Protocol

A set of five specimens is prepared through percussion to generate a flake or by sectioning on a low-speed saw and polishing to a mirror finish. The same piece of obsidian should provide all of the samples. Each specimen is hydrated in a pressure vessel at a specific temperature for a defined length of time. At the end of the time the pressure vessel is cooled rapidly with compressed air or water, the specimen removed, and the hydration rim measured. Hydration is performed either with distilled water (liquid phase hydration), or in a saturated water vapor atmosphere without liquid contact (vapor phase hydration). In liquid phase hydration the water contains a saturated solution of dissolved silica gel to prevent erosion of the glass surface. Temperatures employed in laboratory hydration typically range from $110 - 150^\circ\text{C}$; it has been found the going much over 150°C can lead to diffuse hydration. Hydration times typically range from ten days at the higher temperatures to thirty days or more at the lower temperatures in order to sure that well defined and easily observable hydration layers are present.

Two caveats apply to this method that are related to accuracy and reliability of the resulting rates. First, the accuracy of the method is surprisingly poor unless long hot-soak times are employed. This arises because of the form of equations (25a - c). The best-fit process generates a slope and y-intercept, the latter of which requires extrapolation from the measured values of $1/T$ to zero, which tends to amplify any errors in the data set. Further, equation (26) involves raising the intercept value I to an exponential, which further amplifies errors. The errors in measuring the thickness of the hydration rims seem to be the dominant factor. The effect is reduced by extending the hydration period to achieve larger rims before making the readings; measurement accuracies of $\approx 0.1\mu$ are typically reported by hydration laboratories, so a rim magnitude of 5μ yields a rim CV of 4%, or a rate CV of 10% (Rogers and Stevenson 2019:123, Table 8) Thus, a rim magnitude greater than 5μ is desirable.

The second issue is more serious, and is related to the process of hydration. Hydration involves water molecules penetrating the glass matrix, which causes swelling of the hydrated layer. This swelling, or internal stress, is relieved by a relaxation process that involves a volumetric expansion of the glass, and is a function of glass viscosity (Rogers and Stevenson 2019:122). The relaxation is time-dependent, such that, at a single temperature, the apparent hydration rate varies with time and eventually reached steady state (Rogers and Duke 2014b:433, Fig. 2, 434, Fig. 3; Stevenson and Novak 2011). This essentially invalidates equation (28), which is the basis of the method, so that measuring the hydration rim prior to that settling time gives invalid rates. Rogers and Duke (2014b) found that use of the standard hot-soak protocol yielded inaccurate results for six obsidians from southern Nevada; hydration rates were too large by approximately a factor of two, and the logarithmic Arrhenius plot showed a sigmoid form instead of the expected straight line (Rogers and Duke 2014b:433, Fig. 1).

Between the need to achieve a 5μ rim for a slow hydrating obsidian, and the time for relaxation to settle out, the hot-soak protocol recommended by Rogers and Stevenson (2017:120, Table 2) is as shown in Table 3. Relaxation time is not an issue with archaeologically-formed hydration rims, due to the long hydration times involved.

Table 3. Hot-soak times for laboratory hydration

Temperature, °C	Hot soak time, days. Standard Protocol	Hot soak time, days. Recommended Protocol	Limiting factor
110	30	235	Achieving 5μ rim for a slow obsidian
120	25	120	Achieving 5μ rim for a slow obsidian
130	20	65	Achieving 5μ rim for a slow obsidian, and reaching steady state
140	15	60	Achieving steady state
150	10	55	Achieving steady state

The resulting accuracy in rate is comparable to that achievable with radiocarbon association (Rogers and Stevenson 2017).

Intrinsic Water Calibration

As discussed above, the hydration rate at a given temperature is determined principally by the intrinsic water content of the obsidian and temperature. Geochemical studies have led to equations for the hydration rate of obsidian in terms of temperature, pressure, and intrinsic water

content (Zhang et al. 1991; Zhang and Behrens 2000). However, the data were based on temperatures (400 – 1200°C) and pressures (0.1 – 810 mPa) of interest to volcanology, and the equations do not extrapolate correctly to ambient archaeological temperatures.

Rogers and Stevenson (2021; n.d.) developed an equation relating intrinsic water content and temperature to hydration rate for obsidian in the temperature and pressure ranges typical of archaeology. If intrinsic water content of the specimen is measured, either by IR spectrometry or by mass loss on heating, the hydration rate can be computed for any desired EHT. The equation is based on a least-squares best fit of a mathematical model to a set of published data (N = 29). The model for the temperature dependence is derived from kinetic theory of reactions, and the model for the dependence on water content is based on the mechanics of glass formation. The resulting equation is

$$k = \exp[36.29 - (10005 - 354*w)/T], \quad (32)$$

where k is hydration rate in $\mu^2/1000$ years, w is total structural water content (molecular + hydroxyl) in wt.%, and T is temperature in Kelvins. The equation gives valid hydration rates for archaeological temperatures, with $R^2 = 0.9998$ and accuracy $\approx 0.3427 \mu^2/1000$ years, one-sigma (N = 6). The range of structural water values used in the fit is $0.1 < w < 1.02$ wt.% and the form of the equation conforms with expectations based on the physics of hydration. The wide range of temperatures in the data set (20°C to 180°C) provides a solid basis for verifying the form of the temperature variation.

Use of equation (32) requires knowing w, the intrinsic water content. Measurement techniques for water content are beyond the scope of this paper; spectroscopic methods include Fourier Transform Infrared (FTIR) spectrometry (e.g. Newman et al. 1986; Von Aulock 2014), Infrared Photo-Acoustic Spectrometry (IR-PAS; Stevenson and Novak 2011). An alternative method is to infer water content from density (Ambrose and Stevenson 2004), but has proven to be unreliable in practice.

Curve Re-Fitting

If a best-fit curve is available which does not conform to the known physics discussed here, and if the data from which it was developed are not available, the curve itself can be re-analyzed to provide a rate based on square-root-of-time principles. Describing the method is best done by example.

Basgall and Giambastiani (1995:44) analyzed Queen obsidian artifacts from the Bishop Tablelands area, and computed a best fit equation of

$$t = 82.74*r^{2.06} \quad (33)$$

where t is age in radiocarbon years before the present (rycbp, with “the present” understood as 1950) and r is hydration rim in microns. This equation was apparently the result of a linear best fit to obsidian-radiocarbon data pairs, in which the fit was between $\ln(t)$ and $\ln(r)$. However, the fit does not recognize the physics of the process. Hydration is a diffusion process, and hence, by definition, the exponent in the right side of the equation must be equal to 2, so that equation (1) above applies. The original data set was not published by the researchers, so our re-analysis is based on equation (33).

The analytical procedure was to select a set of hydration rim readings and compute the corresponding age by equation (33); the rim values should be selected to span the likely range of values in the archaeological sample. The ages were then converted to calibrated years before 1950 (cyb1950) using Calib 6.0, and 50 years was added to adjust to the year 2000 (cyb2k). Finally, a linear least-squares best fit was made between r^2 (dependent variable) and t in cyb2k (independent variable). Table 4 presents the data used.

Table 4. Queen obsidian data, Bishop Tablelands.

rim, μ	t, rcybp	t, cyb1950	t, cyb2k
2	345	398	448
4	1439	1353	1403
6	3317	3558	3608
8	5999	6850	6900
10	9500	10824	10874
12	13830	16927	16977
14	18999	22621	22671

The linear best fit constrained to pass through the origin yields a slope of $8.72 \mu^2/1000$ years, which is the rate. The EHT for the project area was computed by regional temperature scaling to be 18.59°C ; adjusting the rate to 20°C yields a rate of $10.34 \mu^2/1000$ years.

In this case the results agree with other methods (Rogers and Stevenson 2019); again, however, the method should be used with care and frequent cross-checking.

Inter-Method Proportionality

This method was developed to compensate for non-equilibrium conditions in certain laboratory induced hydration protocols, as described above and in Rogers and Duke (2014b). A ratio is computed between the non-equilibrium rate and an archaeological rate; it is then applied to correct other laboratory induced hydration rates computed from the same lab protocol, for which archaeological rates are not available. Again, a specific example will be shown.

Rogers and Duke (2014b) reported hydration rates based on laboratory hydration for obsidians from seven Lincoln County, NV, obsidian sources: Meadow Valley Mountains, Delamar Mountains, Panaca Summit, Tempiute Range, Clover Mountains, Wilson Creek Range, and South Pahroc. Hydration rates were also computed based on projectile point data from the Kern River Pipeline for the first three of these sources. The results are in Table 5 (Rogers and Duke 2014b: 433, Table 5).

Table 5. Laboratory and archaeological data for Nevada sources

Source	Induced Rate, $\mu^2/1000$ yrs at 20°C	Archaeological Rate $\mu^2/1000$ yrs at 20°C
Delamar Mountains	31.9	18.3, N = 12
Meadow Valley Mountains	24.3	12.8, N = 27
Panaca Summit	30.2	15.3, N = 93
Tempiute Range	33.8	na
Clover Mountains	19.7	na
Wilson Creek Range	15.2	na
South Pahroc	16.2	na

Further analysis showed that all the induced rates are too high. The physics involved appears to be consistent: in each case the induced hydration rate is clearly not representative of equilibrium conditions, and the logarithmic Arrhenius plots all showed the sigmoid indicating that the relaxation had not reached equilibrium condition under the protocol used. The induced rate is probably the result of an interaction between a transient phenomenon (onset of accelerated hydration at an elevated temperature) and the particular experimental protocol employed.

However, the ratio between archaeological rate and induced rate for the first three sources is very close to the same; for Meadow Valley Mountains it is 0.53, for Delamar Mountains it is 0.57, and for Panaca Summit it is 0.51. The CVs for these rates are large, so the ratios are not statistically distinguishable and we are justified in using the average of 0.54. Thus, the missing archaeological rates can be reconstructed by multiplying the induced rate by 0.54. Since all the specimens were subjected to the same protocol by the lab, the response of the obsidian specimens should be consistent across the various sources, at least to first order, and the fact that the ratios agree so closely for the first three sources is probably not an accident. Applying this method to the remaining four sources yield the rates in Table 6 below.

Table 6. Scaled hydration rate data

Source	Rate, $\mu^2/1000$ yrs at 20°C	Comments
Delamar Mountains	18.3	Archaeological
Meadow Valley Mountains	12.8	Archaeological
Panaca Summit	15.3	Archaeological
Tempiute Range	18.1	Scaled from induced rate
Clover Mountains	10.6	Scaled from induced rate
Wilson Creek Range	8.1	Scaled from induced rate
South Pahroc	8.6	Scaled from induced rate

AGE ACCURACY

There are always errors, or uncertainties, in the parameters used for age computation. In obsidian hydration dating the primary error sources are: obsidian rim thickness measurement; errors in the hydration rate ascribed to a source; intra-source rate variability due to uncontrolled intrinsic water in the obsidian; errors in reconstructing the temperature history (EHT); uncertainties due to humidity variations; and temperature changes caused by site formation processes (Schiffer 1987).

Obsidian sample sizes are generally relatively small due to cost constraints, typically 8-10 specimens, while the uncertainty sources described above produce at least six degrees of freedom in the errors. Thus, sample standard deviation is generally not a good estimate of age accuracy; a better strategy for estimating age accuracy is to use *a priori* information about the individual error sources, and infer the accuracy of the age estimate on this basis. The mathematics to make this inference were developed in Rogers (2010), and are summarized here.

If site formation uncertainty (treated below) is excluded, the coefficient of variation of the computed age estimate can be shown to be

$$CV_t = \text{sqrt}[4*(\sigma_r/r)^2 + (0.12\sigma_{\text{EHT}})^2 + CV_{\text{hum}}^2 + CV_{k_s}^2 + CV_{k_e}^2] \quad (34)$$

where the variables are defined as follows: σ_r is the standard deviation of the hydration rim measurement, and is $\approx 0.1\mu$; r is the measured hydration rim; σ_{EHT} is the standard deviation in EHT post-correction, and is $\approx 1.0^\circ\text{C}$; CV_{ks} is the coefficient of variation of the hydration rate ascribed to the obsidian source; CV_{ke} is the coefficient of variation of rate due to intra-source rate variations; CV_{hum} is the coefficient of variation of rate due to humidity variations. The intra-source intrinsic water variability is by far the largest contributor to age uncertainty, followed by uncertainty in EHT, so CV_{ke} tends to dominate the standard deviation.

Many of the parameters in equation (34) are not accessible to the practicing archaeologist, who usually knows the geochemical source for the specimens, the appropriate hydration rate for that source, and the measured hydration rim, but is not in a position to estimate the error terms. To address this situation, we have derived a simple equation to satisfy the needs of archaeological analysis (Rogers and Yohe 2021). In equation (34) the coefficient of variation of the computed age (CV_t) is composed of the square root of the sum of the squares of five terms: a term quantifying uncertainty due to hydration rim measurement, which varies with the rim value; three terms including uncertainty in EHT, humidity, and ascribed rate, all of which are constant; and a term defining the uncertainty due to intra-source variations in water content, which varies with source. It can be shown from equation (32) that

$$\text{CV}_{\text{ke}} = 1.2 * w * \text{CV}_w \quad (35)$$

Further, obsidian source measurements show that the CV of intrinsic water, CV_w , is in the range of 20 – 40% over a wide range of mean water contents (Rogers and Yohe 2021); if 30% is chosen as a nominal value, equation (35) becomes $\text{CV}_{\text{ke}} = 0.36 * w$. The water content w in turn is related to hydration rate and temperature by equation (32); a linear best fit for between CV_{ke}^2 and k (source hydration rate in $\mu^2/1000$ years at EHT = 20°C) is

$$\text{CV}_{\text{ke}}^2 = 0.007 * k - 0.0763 \quad (36)$$

For the constant term, typical values are $\text{CV}_{\text{EHT}} = 0.11$, $\text{CV}_{\text{hum}} = 0.06$, and $\text{CV}_{\text{ks}} = 0.05$; the constant term is then the sum of the squares, or 0.0182, so the CV of the uncertainty in age, CV_t is

$$\text{CV}_t = \text{sqrt}[(0.16/r_m)^2 + 0.007 * k - 0.0581] \quad (37)$$

Thus, knowing the geochemical source and its associated rate k , and the measured hydration rim r_m for each specimen, the archaeologist can perform EHT adjustments and then compute age by equation (1) and age uncertainty by equation (37). Age standard deviation is then $\sigma_t = t * \text{CV}_t$. Equation (37) agrees with equation (34) to within ± 0.015 rms.

If site formation uncertainty is present, the variance of age due to site formation, VAR_{SF} , can be approximated as

$$\text{VAR}_{\text{SF}} = (t_d - t_s)^2 / 12 \quad (38)$$

where t_d is the age computed for burial depth conditions and t_s is the age computed for surface conditions. Once CV_t is computed from equation (37) or (34), the standard deviation of the age estimate is

$$\sigma_t = t^* \text{sqrt}(CV_t^2 + VAR_{sf}) \quad (39)$$

This is the accuracy figure quoted in the computer program output.

HYDRATION RATES LISTING

Hydration rates are continually being refined as techniques improve, so the rates shown in Table 7 should be regarded as provisional. The analyst should always check on whether the rate employed is giving an archaeologically result that converges with other chronometric information.

Table 7. Provisional hydration rates ($\mu^2/1000$ years at 20°C) for obsidian sources in the eastern California region.

State	Geochemical Source	Rate	Rate CV	E/R, K**	Method*	Remarks
CA	Coso volcanic field (composite)	22.86	0.445	9716	2	
CA	Coso Sugarloaf Mountain	29.87	0.216	9644	1, 4	
CA	Coso West Sugarloaf	18.14	0.190	9786	1, 4	
CA	Coso West Cactus Peak	27.28	0.650	9647	4	
CA	Coso Joshua Ridge	22.27	0.360	9718	4	
CA	Casa Diablo Lookout Mountain	13.04	0.121	9886	5	Small sample
CA	Casa Diablo Sawmill Ridge	12.70	0.113	9893	5	Small sample
CA	Casa Diablo Composite	12.87	0.117	9890	5	Small sample
CA	Bodie Hills	10.38	0.053	9953	4	Small sample
CA	Fish Springs	11.87	0.093	9913	5	
CA	Mono Glass Mountain	16.10	0.184	9824	4	
CA	Mono Craters	33.00	0.398	9614	4	
CA	Saline VI	9.95	0.041	9965	4	Small sample
CA	Eureka Dunes	9.95	0.041	9965	4	
CA	Napa Glass Mountain	10.68	0.062	9944	1	
CA	Obsidian Butte (Salton Sea)	9.09	0.014	9991	2	
NV	Truman-Queen	10.41	0.054	9952	6	
NV	Mt. Hicks	11.79	0.091	9915	4	
NV	Delamar Mountains	18.32	0.223	9786	1,3	
NV	Panaca Summit	15.22	0.167	9840	1,3	
NV	Meadow Valley Mountains	12.79	0.116	9891	1,3	
NV	Tempiute Range	18.10	0.219	9790	7	
NV	Clover Mountains	10.60	0.060	9946	7	
NV	Wilson Creek Range	8.10	0.004	10005	7	
NV	South Pahroc	8.60	0.004	10005	7	
UT	Topaz Mountain	8.14	0.004	10005	1, 2	
UT	Brown's Bench	15.16	0.166	9842	2, 4	

* 1 = laboratory induced hydration; 2 = radiocarbon association; 3 = temporally-sensitive artifact association; 4 = intrinsic water calibration; 5 = artifact baselining; 6 = curve re-fitting; 7 = inter-method proportionality

** Computed by equation (15)

ANALYTICAL PROCEDURE

THE OBSIDIAN HYDRATION DATING PROCESS

Here we describe a recommended process for performing an OHD analysis. The discussion pulls together the mathematics from the preceding text, with practical suggestions for the analysis.

To begin with, the analyst will need the following data to perform an OHD analysis. First, to perform the computations themselves, temperature parameters (either from regional scaling or temperature sensors) and specimen burial depth (cm below the surface) are needed for computation of EHT. The geochemical source of each specimen is needed to match with the hydration rate, and the hydration laboratory report giving rim mean and standard deviation is needed for the age computation; the hydration laboratory comments about hydration layer clarity and thickness variation are especially helpful in evaluating the results and explaining anomalous ages. Next, site nomenclature (trinomial or temporary number) and provenience of each specimen (TU, level, other designation) are needed to report results in a coherent fashion. Tentative identification of each artifact (such as biface, debitage, projectile point) is desirable. Furthermore, if any of the specimens are temporally sensitive, such as projectile points, it is useful to know the typology as a means to cross-check the OHD ages.

Data Preparation

1. Always use geochemical methods to determine obsidian source. Visual sourcing is not reliable at identifying even major sources, such as the Coso volcanic field, and cannot generally identify subsources (such as Coso West Sugarloaf or Coso Joshua Ridge), which may have different hydration rates. If geochemical sourcing was not performed, clearly state the sourcing assumptions made.
2. Group hydration data by geochemical source – never mix sources.
3. Treat obvious tools, such as projectile points or crescents, as individual items ($N = 1$). For the rim standard deviation, use the value reported by the lab.
4. Debitage samples with $N > 1$ may be treated individually or grouped by provenience and burial depth.
5. The hydration rim mean reported by the laboratory is usually the average of six independent readings made on a thin-section, and the reported standard deviation is computed from those six readings. Most labs provide the data in an Excel spreadsheet, with formatting set to round off to one decimal place. It is important to change the formatting to show the standard deviation to three decimal places for the accuracy computation.
6. Tabulate the rim means, standard deviations, burial depths, and geochemical sources for use in the analysis. Explain the rationale for any grouping of data, and especially for any data points excluded (whether by Chauvenet's criterion or judgmentally).

Analysis Procedure – All Sites

1. Compute the site temperature parameters from meteorological records or sensors. A temperature model such as described in Table 2 is a convenient means to do this. If any specimen is from a rock shelter or cave, multiply V_a by 75% and use $V_d = 5^\circ\text{C}$.
2. Make sure all the specimens are matched with the appropriate hydration rate for the geochemical source.
3. Using the temperature parameters from step 1 and the burial depth z in meters, compute the EHT for each specimen by numerical integration of equation (4) or by using equations (6a) and (6b).
4. Compute E/R by equation (10).
5. Compute the EHT-corrected rim thickness for each specimen by equations (7) and (8).

6. Compute ages based on current conditions using equation (1) and the appropriate rate from Table 7 or some other source.
7. Once the ages are known, compute the age standard deviation from equation (34) or (37).

Analysis Procedure – Inclusion of Site Formation Processes

Sites with significant turbation present special problems; examples would be artifacts eroding out of a dune field, or buried artifacts with obvious later alluvial fill over them. In such cases the recovery depth of the artifacts may not reflect the long-term depth, which introduces uncertainty into the temperature history and hence the EHT and hydration rate. Analysis in this case is a judgment call; if such processes are obvious, the recommended procedure for analysis is as follows.

If the age computation is being performed by MS Excel, the procedure is, first, to estimate the fraction of its life the artifact was buried; in the absence of any specific information a default value of 0.5 is recommended. Next the rim correction factors and ages corresponding to the surface and to the recovery depth are computed; the age is then computed by equation (11) and the age standard deviation by equations (38) and (39).

COMPUTATION METHODS

MatLab Code

The analysis code in Appendix B is written in MatLab 7.0, and is compatible with earlier versions of MatLab back to 5.0. The EHT is computed by numerical integration, and age and age standard deviation are computed. The code is fully documented with internal comments, and the variable names are, as far as possible, mnemonic. The code reads input from an MS Excel-generated comma-separated variable (.csv) file, and outputs to a similar file. The user must generate input files, using MS Excel or equivalent. The names on the input and output files may be adjusted by the user. The code and its design are fully documented in Rogers (2018).

MS Excel Workbook

An MS Excel workbook has been developed which follows the procedure outlined above. The workbook contains two worksheets, one for simple cases where site formation processes can be ignored, and one to account for significant site formation processes. The workbook is in an accompanying MS Excel file.

The data in columns A – D in the workbook can be simply copied from the electronic worksheet provided by the obsidian laboratory, and pasted into the workbook. By constructing the workbook with the equations incorporated in the second row (first row of data), the age computation is then carried out by a simple <fill down> procedure in MS Excel. The advantage of such a layout is that it facilitates checking the results, as mistakes show up clearly.

DATA PRESENTATION

In presenting OHD results in a report, always report complete data on the obsidian hydration samples. This should include catalog number or other identifier; a description of the artifact, such as debitage or biface; the mean and standard deviation for each rim; the obsidian source and how it was determined; provenience, including unit designation and burial depth; any unusual circumstances, such as cave or hearth; the EHT-corrected rim means and standard deviations; and the computed mean and standard deviation of the age, in cyb2k. The site

description should always include site elevation.

In presenting data, often multiple specimens must be combined and statistics reported. The mean of the data set is simply the mean of the individual ages; however, the standard deviation of the individual ages is not a good measure of uncertainty, because it ignores the contributions of the individual age standard deviations. Since the standard deviations of the individual ages tend to be large, characterizing a set of ages by the standard deviation of the means is unduly optimistic. The effects of individual standard deviations are included in an aggregate standard deviation σ_a

$$\sigma_a = \text{sqrt}(\sigma_m^2 + B^2) \quad (40)$$

where σ_m is the standard deviation of the mean values of the individual ages and B is the average of the individual specimen variances. This can be easily computed in MS Excel.

CURRENT STATE OF THE OHD ART

It has been 60 years since the original obsidian hydration dating work of Friedman and his colleagues and their work has stood the test of time. They correctly identified the physical process involved (diffusion) and the mathematical form of the hydration law (equation (1) above); they also pointed out, based on physical chemistry, that the diffusion coefficient must be concentration-dependent in order to create a hydration rim. And finally, to their credit, they realized the importance of grouping obsidian by geochemical source, and the effects of temperature and humidity. In succeeding years other researchers, primarily in glass science and geochemistry, developed the field further. The archaeological advances over the past decade, which are the subject of this paper, have been chiefly the result of applying numerical modeling to the known physical and chemical basis of hydration. At present the mechanism of hydration is well understood at a macro level, and can be successfully applied to archaeological problems. Current models enable computing both an age and a standard deviation of the age, and sources of uncertainty contributing to the standard deviation are known.

There are limitations to the current OHD method. We have effective first-order OHD models for effects of intrinsic water, temperature, and humidity; the primary limitations to OHD accuracy and precision occur because these models are generally not developed for the specimen but for the environment. For example, the temperature model is developed for the site and burial depth, but not for the specific obsidian specimen, and humidity can only be accounted for statistically. Similarly, hydration rates are computed for geochemical sources, but do not account for the intrinsic water in a particular obsidian artifact, although the benefits of measuring water content for each specimen have been explored (Rogers and Stevenson 2022). In addition, hydration rates are subject to potential error sources such as the obsidian-radiocarbon association uncertainty. As a result, OHD dates typically have relatively poor precision (age uncertainties of ~ 15 - 25%). Given this modeling process, it is unlikely that further refinement of the present process will lead to dramatic improvements in precision as long as the sources of uncertainty remain unresolved.

OUTLOOK FOR THE FUTURE

Looking to the future, there are four areas of research which promise significant improvements. The first is a method for measuring the intrinsic water content of the individual specimen, cheaply, quickly, and without damage to the specimen. Such a method would enable the hydration rate to be computed for the individual artifact (equation (32)) rather than being ascribed to the geochemical source, and would lead to a dramatic improvement in age precision (Rogers and Stevenson 2022).

A second promising improvement would be a method to determine the temperature history an artifact has experienced by a measurement on the artifact itself, or “intrinsic EHT”. A possible phenomenon is the water speciation process, or refractive index of the specimen. Any EHT thus derived would need to be accurate to $< 1^{\circ}\text{C}$. Much more research is needed in this area.

A third area for research is to develop a quantitative understanding of hydration at the molecular level. The present models, based on diffusion coupled with chemical reaction, are macro-level, phenomenological models; they are based on understanding and including molecular-level effects, but the models themselves are higher-level. The mathematical models of diffusion were first developed in the early 19th century by Laplace, specifically for describing heat transfer in solids; they were subsequently applied to mass transfer by Fick (Crank 1975). For the case of diffusion without reaction and with a constant diffusion coefficient (D in equation (2)) the same results can be derived at the molecular level by kinetic theory (Glicksman 2000:191ff.). This corresponds physically to diffusion of one gas into another without chemical reaction; however, for the more complex case of diffusion with reaction, such a model does not exist. Kuroda et al. (2018) have developed a model at temperatures of $650 - 850^{\circ}\text{C}$ and pressures of 50 bar, but it is not clear that the data extrapolate to archaeological conditions. The goal of research in this area would be a mathematical model which starts with the structure and composition of the glass matrix and allows computing both a hydration rate and the speciation reaction.

A final area of research is much less glamorous, but is sorely needed: a method for measuring the hydration rim without damage to the artifact. Current methods require cutting a small piece of obsidian from the margin of an artifact and are thus regarded as consumptive, and land-management agencies are increasingly unwilling to allow damage to artifacts. (In some cases the notch can be replaced by the unobtrusive removal of a pressure flake, but this still qualifies as consumptive, as does the micron-size pit created by SIMS.). The method would need to be fast, cheap, non-damaging, and applicable to a wide range of artifact types and sizes; a method meeting these criteria does not currently exist.

REFERENCES CITED

- Ambrose, W. R., and C. M. Stevenson
2004 Obsidian Density, Connate Water, and Hydration Dating. *Mediterranean Archaeology and Archaeometry* 4(2):5-16.
- Anovitz, Lawrence M., J. Michael Elam, Lee R. Riciputi, and David R. Cole
1999 The Failure of Obsidian Hydration Dating: Sources, Implications, and New Directions. *Journal of Archaeological Science* 26(7):735-752.
2004 Isothermal Time-Series Determination of the Rate of Diffusion of Water in Pachuca Obsidian. *Archaeometry* 42(2):301-326.
- Anovitz, Lawrence M., David R. Cole, and Mostafa Fayek
2008 Mechanisms of Rhyolitic Glass Hydration Below the Glass Transition. *American Mineralogist* 93:1166-1178.
- Basgall, Mark E.
1990 *Hydration Dating of Coso Obsidian: Problems and Prospects*. Paper presented at the 24th Annual Meeting of the Society for California Archaeology, Foster City.
- Basgall, Mark, and Mark Giambastiani
1995 *Prehistoric Use of a Marginal Environment: Continuity and Change in Occupation of the Volcanic Tablelands, Inyo and Mono Counties, California*. Center for Archaeological Research at Davis, Davis, California.
- Behrens, Harald, and Marcus Nowak
1997 The Mechanisms of Water Diffusion in Polymerized Silica Melts, *Contributions to Mineralogy and Petrology* 126:377-385.
- Bettinger, Robert L.
1989 Establishing an Hydration Rate for Fish Springs Obsidian. In: *Current Directions in California Obsidian Studies*, Richard E. Hughes, ed., pp. 59-68. Berkeley: Contributions of the University of California Archaeological Research Facility No. 48.
- Bintanja, R., R.S.W. van de Wal, and J. Oerlemans.
2005. Modelled atmospheric temperatures and global sea levels over the past million years. *Nature* 437: 125-128, 1 September 2005.
- Campbell, Gaylon
2021 Estimating relative humidity in soil – How to stop doing it wrong. *Environmental Biophysics Corporation* www.environmentalbiophysics.org. doi.org/10.2172/548871
- Carslaw, H. S., and J. C. Jaeger
1959 *Conduction of Heat in Solids*, 2nd ed. Oxford: Clarendon Press.
- Cole, F. W.
1970 *Introduction to Meteorology*. Wiley: New York.
- Crank, J.
1975 *The Mathematics of Diffusion*. Oxford: Oxford University Press.
- Cvetanovic, R. J., D. L. Singleton, and G. Paraskevopoulos
1979 Evaluations of the Mean Values and Standard Errors of Rate Constants and their Temperature Coefficients. *Journal of Physical Chemistry* 83(1):50-60.
- Delaney, J. R., and J. L. Karsten

- 1981 Ion Microprobe Studies of Water in Silicate Melts: Concentration-Dependent Water Diffusion in Silicon. *Earth and Planetary Science Letters* 52:191-202.
- Doremus, R. H.
 1994 *Glass Science*, 2nd. ed. New York: Wiley Interscience.
 2000 Diffusion of Water in Rhyolite Glass: Diffusion-reaction Model. *Journal of Non-Crystalline Solids* 261 (1):101-107.
 2002 *Diffusion of Reactive Molecules in Solids and Melts*. New York: Wiley Interscience.
- Duke, Daron, and Alexander K. Rogers
 2013 Does an Obsidian Hydration Rim Care when a Temperature Fluctuation Occurs? *Bulletin of the International Association for Obsidian Studies* No. 49, Summer 2013, pp. 8-16.
- Ebert, W. L., R. F. Hoburg, and J. K. Bates
 1991 The Sorption of Water on Obsidian and a Nuclear Waste Glass. *Physics and Chemistry of Glasses* 34(4):133-137.
- Everett-Curran, Linda, Richard G. Milo, and Duane Quiatt
 1991 Microgeographic Comparisons of Climate Today Afford Inferences Concerning Past Behavior: An Overview of Data and Applications from a Study of Chapin Mesa (Mesa Verde National Park) Climate. In: *Anasazi Symposium 1991*, Art Hutchinson and Jack E. Smith, eds., pp. 109-116. Mesa Verde: Mesa Verde Museum Association.
- Friedman, Irving, and R. Smith
 1960 A New Method of Dating Using Obsidian; Part 1, the Development of the Method. *American Antiquity* 25 (4):476-522.
- Friedman, Irving, and William Long
 1976 Hydration Rate of Obsidian. *Science* 191(1):347-352.
- Friedman, Irving, Robert I. Smith, and William D. Long
 1966 Hydration of Natural Glass and Formation of Perlite. *Geological Society of America Bulletin* 77:323-328.
- Friedman, I., F. W. Trembour, F. I. Smith, and G. I. Smith
 1994 Is Obsidian Hydration Dating Affected by Relative Humidity? *Quaternary Research* 41(2):185-190.
- Garofalini, Stephen H., Jesse Lenz, and Matthew Homann
 2020 Molecular mechanism of silica glass upon exposure to Moisture. *Journal of the American Ceramic Society* 103:2421-2431.
- Hull, Kathleen L.
 2001 Reasserting the Utility of Obsidian Hydration Dating: A Temperature-Dependent Empirical Approach to Practical Temporal Resolution with Archaeological Obsidians. *Journal of Archaeological Science* 28:1025-1040.
- Hughes, Richard. E.
 1988 The Coso Volcanic Field Reexamined: Implications for Obsidian Sourcing and Dating Research. *Geoarchaeology* 3:253-265.
- Johnson, Michael J., Charles J. Mayers, and Brian J. Andraski
 2002 *Selected Micrometeorological and Soil-Moisture Data at Amargosa Desert Research Site in Nye County near Beatty, Nevada, 1998 – 2000*. U.S. Geological Survey Open-File Report 02-348. USGS, Carson City, Nevada. With CD containing meteorological data records.
- Justice, Noel D.

- 2002 *Stone Age Spear and Arrow Points of California and the Great Basin*. Indiana University Press: Bloomington.
- Karsten, J. R., and J. L. Delaney
1981. Ion microprobe studies of water in silicate melts: concentration-dependent water diffusion in obsidian. *Earth and Planetary Science Letters* 52: 191-202.
- Karsten, J. L., J. R. Holloway, and J. L. Delaney
1982. Ion microprobe studies of water in silicate melts: temperature-dependent water diffusion in obsidian. *Earth and Planetary Science Letters* 59:420-428.
- Kuroda, Minami, Shogo Tachibana, Naoya Sakamoto, Satoshi Okumura, Michihiko Nakamura, and Nisayoshi Yuimoto
2018 Water Diffusion in Silica Glass through Pathways formed by Hydroxyls. *American Mineralogist* 103:412-417.
- Kuroda, Minami, Shogo Tachibana, Naoya Sakamoto, and Hisayoshi Yurimoto
2019 Fast Diffusion Path for Water in Silica Glass. *American Mineralogist* 104:385-390.
- Kuroda, Minami, and Shogo Tachibana
2019 Effect of Dynamical Property of Melt on Water Diffusion in Rhyolite Melt. *ACS Earth and Space Chemistry* 3:2058-2062.
- Lapham, K. E., J. R. Holloway, and J. R. Delaney
1984 Diffusion of H₂O and D₂O in Obsidian at Elevated Temperatures and Pressures. *Journal of Non-Crystalline Solids* 67:179-191.
- Liritzis, Ioannis, and Nikolaos Laskaris
2012 The SIMS-SS Obsidian Hydration Dating Method, In: *Obsidian and Ancient Manufactured Glasses*, Ioannis Liritzis and Christopher M. Stevenson, eds., pp. 26-45. University of New Mexico Press: Albuquerque.
- Mazer, J. J., C. M. Stevenson, W. L. Ebert, and J. K. Bates
1991 The Experimental Hydration of Obsidian as a Function of Relative Humidity and Temperature. *American Antiquity* 56(3):504-513.
- Meyer, S.
1975 *Data Analysis for Scientists and Engineers*. Wiley: New York.
- Morgenstein, Maury E, Carolyn L. Wickett, and Aaron Barkett
1999 Considerations of Hydration-rind Dating of Glass Artefacts: Alteration Morphologies and Experimental Evidence of Hydrogeochemical Soil-zone Pore Water Control. *Journal of Archaeological Science* 26:1193-1210.
- Newman, S., Stolper, E.M., Epstein, S.
1986. Measurement of water in rhyolitic glasses: Calibration of an infrared spectroscopic technique. *American Mineralogist* 71, 1527-1541.
- Pearson, James L.
1995 *Prehistoric Occupation at Little Lake, Inyo County, California: A definitive Chronology*. Unpublished MA thesis, Department of Anthropology, California State University, Los Angeles.
- Riciputi, Lee R., J. M. Elam, L. M. Anovitz, and D. R. Cole
2002 Obsidian Diffusion Dating by Secondary Ion Mass Spectrometry: A Test Using Results from Mound 65, Clalco, Mexico. *Journal of Archaeological Science* 29:1055-1075.
- Ridings, Rosanna
1996 Where in the World Does Obsidian Hydration Dating Work? *American Antiquity* 61(1):136-148.

Rogers, Alexander K.

- 2006 *Hydration Rate of Obsidian: Mathematical Form and Archaeological Implications*. Maturango Museum MS 13, dated November 11, 2006. On File.
- 2007a Effective Hydration Temperature of Obsidian: A Diffusion-Theory Analysis of Time-Dependent Hydration Rates. *Journal of Archaeological Science* 34:656-665.
- 2007b A Tale of Two Gophers: Depth Correction for Obsidian Effective Hydration Temperature in the Presence of Site Turbation Effects. *Bulletin of the International Association for Obsidian Studies*, No. 37, Summer 2007, pp. 7-12.
- 2008a Obsidian Hydration Dating: Accuracy and Resolution Limitations Imposed by Intrinsic Water Variability. *Journal of Archaeological Science*. 35:2009-2016.
- 2008b Field Data Validation of an Algorithm for Computing Effective Hydration Temperature of Obsidian. *Journal of Archaeological Science*. 35:441-447.
- 2008c An Evaluation of Obsidian Hydration Dating as a Chronometric Technique, Based on Data from Rose Spring (CA-INY-372), Eastern California. *Bulletin of the International Association for Obsidian Studies*, No. 40, Winter 2008, pp. 12-32.
- 2010 Accuracy of Obsidian Hydration Dating based on Radiocarbon Association and Optical Microscopy. *Journal of Archaeological Science*. 37: 3239-3246.
- 2011 Do Flow-Specific Hydration Rates Improve Chronological Analyses? A Case Study for Coso Obsidian. *Bulletin of the International Association for Obsidian Studies* No. 45, Summer 2011, pp. 14-25.
- 2012a Temperature Correction for Obsidian Hydration Dating, In: *Obsidian and Ancient Manufactured Glasses*, Ioannis Liritzis and Christopher M. Stevenson, eds., pp. 46-55. University of New Mexico Press: Albuquerque.
- 2012b Estimation of Hydration Rate for Casa Diablo and Fish Springs Obsidians from Tulare Lake Projectile Point Data. Maturango Museum working Manuscript MS109, dated July 1, 2012.
- 2015a An Equation for Estimating Hydration Rate of Obsidian from Intrinsic Water Concentration. *Bulletin of the International Association for Obsidian Studies* No. 53, Summer 2015, pp. 5-13.
- 2015b A Method for Correcting OHD Age for Paleo-temperature Variation. *Bulletin of the International Association for Obsidian Studies* No. 52, Winter 2015, pp. 6-13.
- 2018 A Computer Program in MatLab for Obsidian Hydration Age Computations. *Bulletin of the International Association for Obsidian Studies* No. 59, Summer 2018, pp. 9-18.

Rogers, Alexander K., and Daron Duke.

- 2011 An Archaeologically Validated Protocol for Computing Obsidian Hydration Rates from Laboratory Data. *Journal of Archaeological Science* 38:1340-1345.
- 2014a Estimating Obsidian Hydration Rates from Time-Sensitive Artifacts: Method and Archaeological Examples. *Bulletin of the International Association for Obsidian Studies* No. 51, Summer 2014, pp. 31-38.
- 2014b Unreliability of the Induced Hydration Method with Abbreviated Hot-Soak Protocols. *Journal of Archaeological Science* 52:428-435.
- 2018 *Obsidian Hydration Dating at Bonneville Estates Rockshelter*, paper presented at the 2018 Great Basin Anthropological Conference, Salt Lake City, UT.

Rogers, Alexander K. and Robert M. Yohe II

- 2014 *Obsidian Re-Use at the Rose Spring Site (CA-INY-372), Eastern California: Evidence from Obsidian Hydration Studies*. *Journal of California and Great Basin Anthropology* 34(2):267-280.
- 2016 A Case Study in Site Formation Effects on Obsidian Hydration Dating. *Bulletin of the International Association for Obsidian Studies*, No. 55, Summer 2016, pp. 5-9.
- 2020 Obsidian Hydration Dating of Proposed Paleoindian Artifacts from Tulare Lake, California. *California Archaeology* 12(2):223-239. doi/10.1080/1947461X.2020.1812028
- 2021 An Equation to Compute Accuracy of Obsidian Hydration Dating Ages. *Bulletin of the International Association for Obsidian Studies* No. 67, Winter 2021, pp. 5-14.

Rogers, Alexander K., and Christopher M. Stevenson

- 2017 Protocols for laboratory hydration of obsidian, and their effect on hydration rate accuracy: A Monte Carlo simulation study. *Journal of Archaeological Science: Reports*. 16(2017):117-126.

- 2019 A Hydration Rate for Queen Obsidian, Western Nevada, Based on Density and Water Content. . *Bulletin of the International Association for Obsidian Studies* No. 61, Summer 2019, pp. 24-28.
- 2020 Archaeological Age Computation Based on Obsidian Hydration: A Summary and Current State of the Art. *Bulletin of the International Association for Obsidian Studies* Special Issue No. 63, March 2020, pp. 2-44.
- 2021 Obsidian Hydration Dating with Optical Microscopy: Is Age Accuracy Improved by Measuring Structural Water Content of a Specimen? *Bulletin of the International Association for Obsidian Studies* No. 68, Summer 2022, pp. 8-23.
- n.d. An Equation Relating Obsidian Hydration Rate to Temperature and Structural Water Content. *Bulletin of the International Association for Obsidian Studies*. In press.
- Schiffer, M. E.
1987 *Site Formation Processes of the Archaeological Record*. Salt Lake City: University of Utah Press.
- Shelby, John E.
2005 *Introduction to Glass Science and Technology*, 2nd. ed. Royal Society of Chemistry: Cambridge.
- Smith, Geoffrey M., Pat Barker, Eugene Hattori, and Ted Goebel
2013 Points in Time: Direct Radiocarbon Dates on Great Basin Projectile Points. *American Antiquity* 78(3):580-594.
- Steffen, Anastasia
2005 *The Dome Fire Obsidian Study: Investigating the Interaction of Heat, Hydration, and Glass Geochemistry*. PhD dissertation, University of New Mexico.
- Stevenson, Christopher M., and Barry E. Scheetz
1989 Induced Hydration Rate Development of Obsidians from the Coso Volcanic Field: A Comparison of Experimental Procedures. In: *Current Directions in California Obsidian Studies*, Richard E. Hughes. ed., pp. 23-30. Berkeley: Contributions of the University of California Archaeological Research Facility No. 48.
- Stevenson, Christopher M., E. Knauss, J. J. Mazer, and J. K. Bates
1993 The Homogeneity of Water Content in Obsidian from the Coso Volcanic Field: Implications for Obsidian Hydration Dating. *Geoarchaeology* 8(5):371-384.
- Stevenson, Christopher M., J. J. Mazer, and B. E. Scheetz
1998 Laboratory Obsidian Hydration Rates: Theory, Method, and Application. In: *Archaeological Obsidian Studies: Method and Theory. Advances in Archaeological and Museum Science*, Vol. 3, M. S. Shackley, ed., pp.181-204. New York: Plenum Press.
- Stevenson, Christopher M., Mike Gottesman, and Michael Macko
2000 Redefining the Working Assumptions for Obsidian Hydration Dating. *Journal of California and Great Basin Anthropology* 22(2):223-236.
- Stevenson, C. M., I. M. Abdelrehim, and S. W. Novak
2004 High Precision Measurement of Obsidian Hydration Layers on Artifacts from the Hopewell Site Using Secondary Ion Mass Spectrometry. *American Antiquity* 69(4):555-568.
- Stevenson, Christopher M., and Steven W. Novak
2011 Obsidian Hydration Dating by Infrared Spectroscopy: Method and Calibration. *Journal of Archaeological Science* 38:1716-1726.
- Stevenson, Christopher M., and Alexander K. Rogers
2014 Transient and Equilibrium Solubility of Water in Rhyolitic Glass: Implications for Hydration Rate Development at Elevated Temperature. *Journal of Archaeological Science* 45:15-19.
- Stevenson, Christopher M., Alexander K. Rogers, and Michael D. Glasscock

- 2019 Variability in Structural Water Content and its Importance in the Hydration Dating of Cultural Artifacts. *Journal of Archaeological Science: Reports* 23:231-242.
- Taylor, John R.
1982 *An Introduction to Error Analysis*. Mill Valley: University Science Books.
- Von Aulock, F. W., B. M. Kennedy, C. I. Schipper, J. M. Castro, D. E. Martin, C., Oze, J. M. Watkins, P. J. Wallace, L. Puskar, F. Begue, A. R. L. Nichols, H. Tuffen
2014 Advances in Fourier Transform Infrared Spectroscopy of Natural Glasses: From Sample Preparation to Data Analysis. *Lithos* 206-207:pp. 53-64.
- West, G. J., W. Woolfenden, J. A. Wanket, and R. S. Anderson
2007 Late Pleistocene and Holocene Environments. In: *California Prehistory: Colonization, Culture, and Complexity*, T. L. Jones and K. A. Klar, eds., pp. 11-34. Altamira Press: Walnut Creek.
- Yohe, Robert M. II
1992 *A Reevaluation of Western Great Basin Cultural Chronology and Evidence for the Timing of the Introduction of the Bow and Arrow to Eastern California based on new Excavations at the Rose Spring Site (CA-INY-372)*. Unpublished PhD Dissertation, Department of Anthropology, University of California, Riverside.
1998 The Introduction of the Bow and Arrow and Lithic Resource Use at Rose Spring (CA-INY-372). *Journal of California and Great Basin Anthropology* 20(1):26-52.
- Zhang, Youxue
2008 *Geochemistry*. Princeton University Press
- Zhang, Y., E. M. Stolper, and G. J. Wasserburg
1991 Diffusion of Water in Rhyolytic Glasses. *Geochimica et Cosmochimica Acta* 55:441-456.
- Zhang, Youxue, R. Belcher, L. Wang, and Sally Newman
1997 New Calibration of Infrared Measurement of Dissolved Water in Rhyolytic Glasses. *Geochimica et Cosochemica Acta* 62:3089-3100.
- Zhang, Y, and H. Behrens
2000 H₂O Diffusion in Rhyolytic Melts and Glasses. *Chemical Geology* 169:243-262.

APPENDIX A.
MATHEMATICAL THEORY OF DIFFUSION

The obsidian hydration process is modeled physically as a diffusion-reaction process in a homogeneous medium in one dimension, described by the partial differential equation

$$\partial C/\partial t = \partial/\partial x (D\partial C/\partial x) - \partial S/\partial t, \quad (\text{A-1})$$

where C is concentration of diffusing molecular water, t is time, D is the diffusion coefficient, S is the concentration of water molecules which have reacted with the glass matrix, and x is depth into the glass.

As applied to hydration, the curve for C defines the concentration of molecular water as a function of depth and time. If the hydration rim, or observable region, is defined as a particular point on the curve of C vs. depth, then that point progresses according to the equation

$$x^2 = D*t \quad (\text{A-2})$$

which is the familiar form of the obsidian hydration equation.

However, in the archaeological case D is not actually constant, since it is a strong function of temperature through the familiar Arrhenius equation for reaction kinetics,

$$D = A \exp [-E/(R*T)]. \quad (\text{A-3})$$

Here A is a constant with units of [length²/time], E is the activation energy of the diffusion reaction in J/mol, R is the universal gas constant (8.314 J/mol °K), and T is absolute temperature in °K. Thus, since the temperature undergoes both annual and diurnal variation, D varies as well.

If D is a function of time only, a solution can be developed by a substitution of variables technique (see Crank 1975, pp. 104-105). The resulting hydration rim equation, analogous to equation (3), is,

$$r^2 = D_{\text{eff}} * t, \quad (\text{A-4})$$

where rim thickness r is substituted for x, and D_{eff} is the archaeological hydration rate, referred to as k in equation (1), and defined by

$$D_{\text{eff}} = (1/t) \int D(t') dt'. \quad (\text{A-5})$$

Thus, if the value of D_{eff} is computed for a time-varying temperature, age can be estimated from equation (A-4). Substituting equation (A-3) into equation (A-5) allows computation of D_{eff},

$$D_{\text{eff}} = (1/t) A \int \exp\{E/[RT(t')]\} dt', \quad (\text{A-6})$$

with $T(t)$ defining the time variation of temperature. Since no closed-form solution to this integral is known, it must be solved numerically as a finite sum:

$$D_{\text{eff}} = (1/N) \sum A \exp\{E/[RT(t_i)]\}, \quad (\text{A-7})$$

with the sum being taken over the hydration time in N increments of $\Delta t = t_{i+1} - t_i$. An effective hydration temperature T_e (or EHT) can be defined by substituting D_{eff} into equation (A-3):

$$T_e = E/[R \ln(D_{\text{eff}}/A)]. \quad (\text{A-8})$$

If a time-varying temperature history can be modeled numerically, equation (A-7) can be used to compute an effective hydration rate constant, and an effective hydration temperature can then be computed by equation (A-8). The resulting EHT is a rigorous solution for time-varying D .

Eliminating D_{eff} between equations (A-7) and (A-8), substituting EHT for T_e , and rearranging terms, the effective hydration temperature is

$$\text{EHT} = -(E/R)/\ln\{(1/N) \sum \exp\{E/[R \cdot T(t_i)]\}\}. \quad (\text{A-9})$$

The sum in equation (A-9) is taken over at least one full cycle of the lowest-frequency variation (twelve months, in the archaeological case).

Equation (A-9) is important as the basis for computing EHT, which in turn is the basis for controlling for temperature in OHD. *Effective hydration temperature, defined by equation (10), is a single temperature which yields the same hydration results as the actual varying temperature over the same time.* Due to the mathematical form of the dependence of hydration rate on temperature (equation [A-3]), EHT is always higher than the mean temperature (except in the uninteresting case of a constant temperature, in which case they are the same).

Further discussion and details are in Rogers (2007a, 2012).

APPENDIX B AGE ANALYSIS CODE LISTING (MatLab)

```

% Program OHDCODEBL21
% Update 11/14/2021
% Obsidian hydration analysis code baseline. Computes age in cyb2k & age
accuracy.
% Characteristics: Matrix I/O, lines 27 and 219.
% EHT by numerical integration for current conditions in SW Great Basin.
% Computes activation energy from inferred water content.
% Rates updated per SCA2022 paper.
% Diurnal variation amplitude represented by cosine model.
% Updated with Nov 2021 error model.
% Bypasses specimens with zero rim.
%
%*****
%
% Module 1 - set constants
clear
YBZ = 0.5; % Default value of fraction of time artifact was at depth
EHTR = 20.0; % Reference EHT for hydration rates, deg C
EHTRK = EHTR + 273.15; % Reference EHT for hydration rates, deg K
%
%*****
%
% Module 2 - Read input data from a .csv file
INDATA = csvread('C:\MATLAB701\work\SilverPeakIn.csv');
L = size(INDATA,1);
for jj = 1:L % j is index for sequence number.
    No = INDATA(jj,1); %No = Sequence Number
    alt = INDATA(jj,2); %alt = Altitude of archaeological site, ft
    rim = INDATA(jj,3); %rim = Uncorrected rim thickness, microns
    sig = INDATA(jj,4); %sig = Rim standard deviation, microns
    z = INDATA(jj,5)/100; %z = Burial depth of artifact, meters
    FL = INDATA(jj,6); %FL = Obsidian source flow:
    % SLM=1, WSL=2, WCP=3, JRR=4, BH = 5, CDSR = 6, CDLM = 7, Queen =8,
    % NGM = 9, Fish Springs = 10, Obs Butte = 11, Saline V1 = 12
    % Mono Glass Mtn = 13, Casa Diablo Composite = 14
    NS = 1; % Sample size
    NOM = 2; % Nominal condition flag; 1 = surface, 2 = mixed, 3 = depth
%
%*****
%
% Module 3 - Compute obsidian parameters from hydration rate
%
% Parameters for aggregate Coso volcanic field
    ratecal = 22.86;
    w = .816;
% Default rate for Coso volcanic field, u^2/1000 yrs @ 20 deg C
% Set parameters for individual flows
    if FL == 1 % SLM
        ratecal = 29.87;
        w = 1.02;
    end
    if FL == 2 % WSL
        ratecal = 18.14;

```

```

    w = 0.62;
end
if FL == 3 % WCP
    ratecal = 27.28;
    w = 1.01;
end
if FL == 4 % JRR
    ratecal = 22.27;
    w = 0.81;
end
if FL == 5 % Bodie Hills
    ratecal = 10.38;
    w = 0.161;
end
if FL == 6 % Casa Diablo Sawmill Ridge
    ratecal = 12.70;
    w = 0.31;
end
if FL == 7 % Casa Diablo Lookout Mtn
    ratecal = 13.04;
    w = 0.33;
end
if FL == 8 % Queen
    ratecal = 10.41;
    w = 0.14;
end
if FL == 9 % Napa Glass Mtn
    ratecal = 11.68;
    w = 0.16;
end
if FL == 10 % Fish Springs
    ratecal = 11.87;
    w = 0.25;
end
if FL == 11 % Obsidian Butte
    ratecal = 9.09;
    w = 0.02;
end
if FL == 12 % Saline V1
    ratecal = 9.95;
    w = 0.10;
end
if FL == 13 % Mono Glass Mountain
    ratecal = 16.10;
    w = 0.10;
end
if FL == 14 % Casa Diablo Composite
    ratecal = 12.87;
    w = 0.32;
end
ageconst = 1000/ratecal;
% Compute E/R
EoverR = 10433-1023*w; % deg K
%
%*****
%
% Module 4 - Temperature model

```

```

% Compute temperature parameters for site.
  STA  = 22.71 - 0.002*alt; % Annual Average temperature
  SVA  = 24.25 - 0.0006*alt; % Annual temperature variation, surface
  SVDM = 18.49 - 0.0007*alt; % Mean diurnal variation, surface
  SVDAM = 2.08; % Amplitude of diurnal variation, surface.
%
%*****
  AGE = 0;
  MODSD = 0;
  SFSD = 0;
  MODCV = 0;
  if rim > 0;
% Module 5 - Compute Keff and EHT
% EHT at the surface
  DIUP = 2*pi/24; %diurnal period in radians/hour
  ANNP = 2*pi/(24*365); % annual period in radians/hour
  Nyears = 1; % Length of integration period, years
  MM = Nyears*365*24; % Number of data points to integrate
  Kint = 0;
  for I = 1:MM
    SVD = SVDM + SVDAM*cos(ANNP*I);
    k = exp(-EoverR/((STA+273.15) + (0.5*SVD*cos(DIUP*I))+
(0.5*SVA*cos(ANNP*I))));
    Kint = Kint + k;
  end
  Keffsurf = Kint/MM;
  EHTKS = -EoverR/(log(Keffsurf)); % EHT in deg K at surface
  EHTCS = EHTKS - 273.15; % EHT at surface in deg C
  if z > 0
% Conditions at depth
    SVAB = SVA*exp(-0.44*z); % Annual variation @ artifact recovery
depth
    Kint = 0;
    for I = 1:MM
      SVDB = (SVDM + SVDAM*cos(ANNP*I))*exp(-8.5*z); % Diurnal
variation @ artifact recovery depth
      k = exp(-EoverR/((STA+273.15) + (0.5*SVDB*cos(DIUP*I))+
(0.5*SVAB*cos(ANNP*I))));
      Kint = Kint + k;
    end
    Keff = Kint/MM;
    EHTKD = -EoverR/(log(Keff)); % EHT at artifact depth, deg K
    EHTCD = EHTKD-273.15; % EHT at artifact depth, deg C
    % Compute effective K and EHT for artifact buried YB fraction of
its life.
    Keffaverage = (1-YBZ)*Keffsurf+YBZ*Keff;
    EHTKA = -EoverR/log(Keffaverage); % Average EHT, deg K
  end
%
%*****
%
% Module 6 - Age computation
  TEMPFACR = EoverR/EHTRK; % Temperature factor, reference conditions
% Surface conditions
  TEMPFACS = EoverR/EHTKS; % Temperature factor
  RCFS = exp((-TEMPFACR+TEMPFACS)/2); %Rim correction
  rimprimeS = rim*RCFS; % Rim corrected to rate EHT

```

```

t1S = ageconst*rimprimeS^2; % Age
AGE = t1S; % Output variable
RIMPRIME = rimprimeS;
SDPRIME = sig*RCFS;
if z > 0
% Conditions at depth
    TEMPFACD = EoverR/EHTKD; % Temperature factor
    RCFD = exp((-TEMPFACR+TEMPFACD)/2); % Rim correction
    rimprimeD = rim*RCFD; %Rim corrected to reference EHT
    t1D = ageconst*rimprimeD^2; % Age at depth conditions
    % Conditions for artifact buried YB fraction of time
    TEMPFACA = EoverR/EHTKA; % Temperature factor
    RCFA = exp((-TEMPFACR+TEMPFACA)/2); % Rim correction factor
    rimprimeA = rim*RCFA; % Rim corrected to reference EHT
    t1A = ageconst*rimprimeA^2; % Age
    rimprimeD = rimprimeA;
    AGE = t1A; % Output variable
    RIMPRIME = rimprimeA;
    SDPRIME = sig*RCFA; % EHT corrected rim SD
end
%
%*****
%
% Module 7 - Source/process model standard deviation
    MODCV = sqrt((0.16/rim)^2+0.007*ratecal-0.0581);
    MODSD = AGE*MODCV;
    if z > 0;
        SFSD = abs(t1S-t1D)/sqrt(12); % Age uncertainty std dev due to site
formation processes
        SFCV = SFSD/AGE; % Additional age CV due to site formation
        MODSD = AGE*sqrt(MODCV^2+SFCV^2); % Std dev of age including SF
        MODCV = MODSD/AGE; % CV of age including SDF
    end
end
%
%*****
%
% Module 8 - Output data as .csv file
OUTDATA(jj,1) = No; % sequence no.
OUTDATA(jj,2) = alt; % site altitude, ft
OUTDATA(jj,3) = STA; % Annual temp, deg C
OUTDATA(jj,4) = SVA; % Annual variation, deg C
OUTDATA(jj,5) = SVDM; % Mean diurnal variation, deg C
OUTDATA(jj,6) = EHTCS;% EHT on surface
OUTDATA(jj,7) = rim; % uncorrected rim mean, microns
OUTDATA(jj,8) = sig; % Uncorrected rim sd, microns
OUTDATA(jj,9) = z*100; % artifact burial depth, cm
OUTDATA(jj,10)= FL; % Obsidian flow
OUTDATA(jj,11)= RIMPRIME; %EHT corrected rim mean
OUTDATA(jj,12)= SDPRIME; % Rim SD, corrected for EHT
OUTDATA(jj,13)= AGE; % Age, years
OUTDATA(jj,14)= MODSD; % Source/process SD of age, yrs +/-
OUTDATA(jj,15)= SFSD; % Age std dev due to site formation processes
OUTDATA(jj,16)= MODCV; % Age CV including SF
end
dlmwrite('SilverPeakOut.csv', OUTDATA, ',')
fprintf('Run Complete')

```

APPENDIX C
TIME AVERAGING OF HYDRATION RATE WHEN SITE FORMATION
PROCESSES ARE SIGNIFICANT; DERIVATION OF THE METHOD

This derivation is mathematically identical to the process programmed in MatLab, in that both compute a time average of the hydration rate for two different depths. The difference is that, in MatLab, the EHT is computed by numerical integration over the temperature history model; the analysis here can be applied to EHT computed by the algebraic best fit, equations (6a – b).

Assume an artifact is recovered from a depth z , but examination of the stratigraphy suggests that major turbation has occurred, such that the artifact was probably buried for Y fraction of its life and on the surface for $1 - Y$ fraction. Further assume the artifact has a measured hydration rim r_m , and is known to have a hydration rate of k_m for the (unknown) EHT it has experienced. This EHT is unknown, but lies between the EHT for the surface and the EHT for the burial depth. By equation (1) the age of the specimen is then

$$t = r_m^2/k_m \quad (C-1)$$

Then by time-averaging the rate k_m is

$$k_m = [Y*k_d + (1 - Y)*k_s] \quad (C-2)$$

Equation (7) gave a rim correction factor (RCF) to adjust hydration rims to the EHT of the rate. The corresponding equation for adjusting the rate is

$$RF_x = \exp\{(E/R)/(EHT_z + 273.15) - (E/R)/(EHT_x + 273.15)\} \quad (C-3)$$

where EHT_z is the EHT for the hydration rate at reference conditions (such as 20°C) and EHT_x is the EHT for either the surface or the burial depth. Note that the factor of 2 no longer occurs in the exponential, and the signs are reversed. Put another way, equation (C-3) adjusts the rate at reference conditions to what it would be at the surface or at depth. Therefore, at the surface ($x = s$) the rate is

$$k_s = k_z*RF_s \quad (C-4a)$$

and at depth ($x = d$) the rate is

$$k_d = k_z*RF_d \quad (C-4b)$$

where k_z is the rate at reference conditions. Then by equation (C-2)

$$k_m = k_z*[Y*RF_d + (1 - Y)*RF_s] \quad (C-5)$$

Further, since $RF = 1/RCF^2$, if the rim corrections have already been computed, the age estimate is

$$t = r_m^2 / \{k_z * [Y/RCF_d^2 + (1 - Y)/RCF_s^2]\} \quad (C-6)$$

The square root of the reciprocal of the denominator is the effective rim correction factor, including rate averaging, RCF_{eff}

$$RCF_{eff} = \text{sqrt}(1/[Y/RCF_d^2 + (1 - Y)/RCF_s^2]) \quad (C-7)$$

so the age estimate is

$$t = (r_m * RCF_{eff})^2 / k_z \quad (C-8)$$

In many cases it is not possible to assign a value to Y with any degree of certainty, so a useful default is $Y = 0.5$ (i.e. half the time). For this case the effective rim correction factor is

$$RCF_{eff} = [1/RCF_d^2 + 1/RCF_s^2]/2 \quad (C-9)$$

Equations (C-7) and (C-9) yield ages which are slightly older than the simple arithmetic average of t_s and t_d .